Monthly Notices
of the
ROYAL ASTRONOMICAL SOCIETY

MNRAS **454,** 64–82 (2015) doi:10.1093/mnras/stv1915

Tidal downsizing model – I. Numerical methods: saving giant planets from tidal disruptions

Sergei Nayakshin★

Department of Physics & Astronomy, University of Leicester, Leicester, LE1 7RH, UK

Accepted 2015 August 18. Received 2015 August 3; in original form 2014 November 19

ABSTRACT

Tidal downsizing (TD) is a recently developed planet formation theory that supplements the classical gravitational instability (GI) disc model with planet migration inward and tidal disruptions of GI fragments in the inner regions of the disc. Numerical methods for a detailed population synthesis of TD planets are presented here. As an example application, the conditions under which GI fragments collapse faster than they migrate into the inner $a \sim$ a few AU are considered. It is found that most gas fragments are tidally or thermally disrupted unless (a) their opacity is ∼3 orders of magnitude less than the interstellar dust opacity at metallicities typical of the observed giant planets, or (b) the opacity is high but the fragments accrete large dust grains (pebbles) from the disc. Case (a) models produce very low mass solid cores ($M_{\rm core} \lesssim 0.1\,{\rm M}_\oplus$) and follow a negative correlation of giant planet frequency with host star metallicity. In contrast, case (b) models produce massive solid cores, correlate positively with host metallicity and explain naturally while giant gas planets are overabundant in metals. Present paper does not address survival of giant planets against rapid migration into the host star, a question which is addressed in two follow-up papers.

Key words: Planets and satellites: formation – planets and satellites: gaseous planets – planet – disc interactions.

1 INTRODUCTION

A planet is a self-gravitating object composed of a heavy element core and an envelope of gas. Terrestrial-like planets are dominated by solid cores whereas giant gas planets are mainly hydrogen gas. There are two competing scenarios for planet formation that take opposite views on what comes first (for a recent review see Helled et al. 2014). In the top-down scenario hydrogen gas cloud comes first and the solid element core is assembled later. In the bottom-up picture, the solid core must be made first before a bound gas envelope appears. In the former scenario planets *loose* mass (gas), as they mature, whereas in the latter planets gain mass with time.

The top-down hypothesis takes roots in the Kuiper (1951) proposition that planets begin their existence as self-gravitating condensations of ∼3 $M_{\rm J}$ of gas and dust formed in the solar nebula by gravitational instability (GI) of the disc (see also Cameron 1978). McCrea & Williams (1965) showed that microscopic grains grow and sediment to the centre of such gas clumps within a few thousand years, presumably forming a massive solid core there (cf. also Boss 1997, 1998). These cores are the seeds of terrestrial-like planets in the model. Kuiper (1951) and McCrea & Williams (1965) proposed that these cores could be all that is left of the original gas protoplanets if the dominant gas component is disrupted by tidal forces from the Sun (this process was rediscovered by Boley et al. 2010). It is natural in this picture that giant planets in the Solar system are further away from the Sun than rocky ones.

On the other hand, Safronov (1972) instead posited that microscopic dust grains in the protoplanetary disc grow larger and then collect into rocks of at least ∼1 km size, called planetesimals. These coalesce into even larger solid cores. Low-mass cores become terrestrial planets. Largest cores, of mass $M \gtrsim 10\,{\rm M}_\oplus$ (10 Earth masses), attract gaseous atmospheres from the protoplanetary disc and end up as giant gas planets (e.g. Pollack et al. 1996). This bottom-up scenario is now called core accretion (e.g. Alibert et al. 2005; Mordasini, Alibert & Benz 2009) and is by far the most popular planet formation theory.

Differentiation between these two theories was thought to be straight forward based on the Solar system data. GI unstable discs were argued not to produce self-gravitating clumps at all at the location of the Solar system planets due to an inefficient disc cooling (Gammie 2001; Rafikov 2005; Rice, Lodato & Armitage 2005), so the sequence of events envisioned by the top-down picture could not be even started. Core Accretion (CA) picture, on the other hand, proved quite successful in explaining the Solar system (Pollack et al. 1996; Tsiganis et al. 2005).

However, the above criticism of the top-down scenario neglects the possibility of planet migration, that is, shrinking of the planet's

★ E-mail: sergei.nayakshin@astro.le.ac.uk

orbit due to gravitational torques from the protoplanetary disc (e.g. Lin & Papaloizou 1979; Goldreich & Tremaine 1980; Lin, Bodenheimer & Richardson 1996). Boley et al. (2010) and Nayakshin (2010a) pointed out that gravitationally unstable discs do not actually need to form gas clumps at ∼ a few AU to explain the observed planets there: in simulations, most GI fragments are found to migrate rapidly from their birth locations at ∼100 AU into the inner disc (e.g. Vorobyov & Basu 2006; Baruteau, Meru & Paardekooper 2011; Cha & Nayakshin 2011; Zhu et al. 2012). It is hence plausible that all of the observed giant planets were hatched by GI in the outer disc and were then pulled much closer to the host star by the gravitational disc torques. Furthermore, some of the fragments could give birth to Earth-mass or more massive cores by grain growth and sedimentation, and be tidally disrupted, potentially providing a 'new' pathway[1] to forming all kinds of planets at all separations in a single framework that was called 'tidal downsizing' (TD).

Bowler et al. (2015) recently presented the results of the Planets Around Low-Mass Stars (PALMS) survey which shows that the frequency of giant gas planets at large separations (∼10–100 AU) is very low, e.g. less than ∼10 per cent, implying that the 'poster child' GI-planet system HR 8799 (Marois et al. 2008) is very rare. Bowler et al. (2015) conclude that 'disc instability is not a common mode of giant planet formation'. In the context of TD hypothesis, the observations of Bowler et al. (2015), unfortunately, do not tell us directly about disc fragmentation properties at these separations; they rather show that GI planets rarely survive at their initial large separations to the present day. In fact, given that the inwards migration times of GI planets are as short as ∼0.01 Myr (Baruteau et al. 2011), it has been argued that it is not clear how any of the observed GI planets (such as the multiplanetary system HR 8799) survive. For example, Zhu et al. (2012) found that all of their 13 simulated gas clumps were either tidally destroyed, migrated into the inner few AU, or became brown dwarfs due to gas accretion. Observations of Bowler et al. (2015) are therefore in excellent agreement with expectations of TD. Any GI model that does not include migration of planets should be treated with suspicion at this day and age when an extremely rapid migration of giant planets in self-gravitating accretion discs has been confirmed by around a dozen independent research teams (to add to the references above, see also Mayer et al. 2004; Machida, Inutsuka & Matsumoto 2010; Michael, Durisen & Boley 2011; Nayakshin & Cha 2013; Tsukamoto et al. 2015).

The first population synthesis model for TD hypothesis was presented by Forgan & Rice (2013b), who used a semi-analytical approach to disc evolution and an analytical description for fragment contraction, grain growth and the resultant core formation. The results of their study are not particularly encouraging for TD. Many fragments were found to run away in mass by accreting gas and became brown dwarfs at large separations from the parent star. Others were disrupted by tides before they could assemble a massive core. While solid cores with masses up to ∼10 $M_\oplus$ were assembled inside the fragments by grain sedimentation, most of them were locked inside brown dwarf mass fragments. Out of a million gas fragments simulated, only one yielded an Earth mass core *without* an overlaying massive gas envelope. More recently, population synthesis was also performed by Galvagni & Mayer (2014), who used different prescriptions for fragment cooling and did not address core formation. In contrast to Forgan & Rice (2013b), the latter study found that most of the gas fragments yield hot Jupiters rather than brown dwarfs at large separations.

This large difference in the results of the two studies motivates the present paper, which improves on both by using 1D numerical rather than analytical descriptions of the coupled disc and planet evolution. While a detailed comparison to the data is to be reported in follow-up publications, as a way of illustrating the methods, the question of GI fragments surviving the initial rapid inwards migration from their birth place into the inner disc regions is considered. To become a present day planet observable by the radial velocity or the transit method, the fragment must not only survive the migration phase from ∼100 AU to the inner few AU, but should also stop migrating inwards before the disc is dissipated. This important issue is not addressed here, but is considered in Paper II and Paper III (Nayakshin & Fletcher 2015).

Giant planets are observed to be much more frequent around metal-rich stars than around metal-poor ones (Gonzalez 1999; Fischer & Valenti 2005). This correlation has been argued to provide a direct support to CA theory (e.g. Ida & Lin 2004, 2008; Mordasini et al. 2009). At the same time, GI planets (and thus TD planets also) are expected to survive the inwards migration phase most readily in metal-poor environments because their radiative cooling is the fastest at low dust opacities (Helled & Bodenheimer 2011). This therefore appears to contradict the observed planet-metallicity correlation and is a very clear challenge to the TD hypothesis.

Accretion of 'pebbles', ∼0.1–10 cm sized grains, from the surrounding protoplanetary disc on to solid bodies, e.g. large planetesimals up to massive cores, has been studied by a number of authors (e.g. Johansen & Lacerda 2010; Ormel & Klahr 2010; Lambrechts & Johansen 2012, 2014; Johansen et al. 2014). Nayakshin (2015a) argued that while pre-collapse giant planets may be inefficient gas accretors (see Section 2.4 further on this), they nevertheless should accrete pebbles for same reasons as solid cores in the CA picture do, except at higher rates because TD fragments have much higher (∼1 Jupiter) masses. Adding a pebble injection term to the equations of an otherwise isolated TD fragment evolution, a surprising result was obtained: the fragments actually accelerated their contraction and collapsed sooner, not later, despite the increase in the dust opacity associated with the higher metallicity of the fragments. Nayakshin (2015a) explained the effect in terms of the extra weight and (negative, of course) potential energy that pebbles bring with them into the gas fragments. Pre-collapse fragments turn out to be very sensitive to pebble accretion because they are nearly polytropes with low effective adiabatic indexes, $\gamma \approx 1.4$. It was found that addition of ∼10 per cent by mass in grains is sufficient to drive a typical pre-collapse molecular H fragment into collapse.

Nayakshin (2015b) presented a population synthesis like study that included the 'metal overload' collapse due to pebble accretion on TD planets for the first time, and found a strong positive rather than negative correlation of giant planet survival with disc metallicity. His model did not include the processes of grain growth, sedimentation and core formation inside the fragment.

This paper expands the work of Nayakshin (2015b) by adding core growth processes. Further, two ways of enhancing the survived giant planet fraction are considered: pebble accretion and lower dust opacity due to grain growth. It is argued that low opacity models require unrealistically small dust opacities (∼3 orders of magnitude smaller than the interstellar grain opacity at same metallicity) to save the gas fragments from disruptions.

The paper is structured as following. A brief introduction into the TD hypothesis and relevant literature is given in Section 2 below.

[1] The author of this article, embarrassingly, did not know of the Kuiper (1951) and McCrea & Williams (1965) suggestions until they were pointed out to him by I. Williams after a seminar at the Queen Mary University in the fall of 2010.

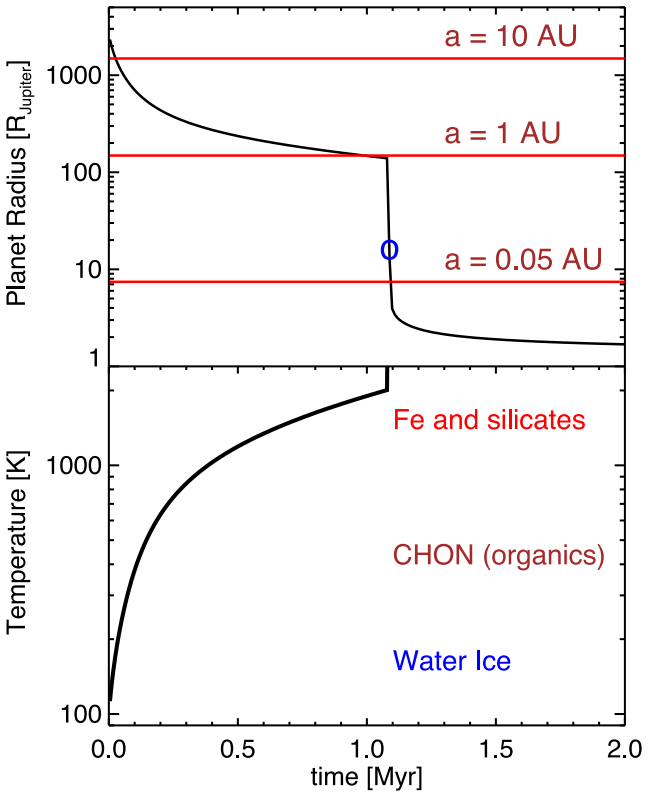

Figure 1. Radiative cooling of an isolated Jupiter mass gas giant planet. The planet is coreless and of solar composition. The upper panel shows planet's radius (black curve). The three horizontal lines depict the planet's Hill radius if the planet were in orbit around a 1 $M_\odot$ mass star at distances indicated just above the lines. The lower panel shows evolution of the central temperature of the planet. During the first million years, the planet is dominated by molecular hydrogen. The three different grain species considered here condense out below temperatures indicated approximately by the location of the species name in the panel.

Numerical algorithms for simulating the planet–disc interaction and the disc evolution are presented in Section 3. Section 4 deals with the methods used to calculate the fragment evolution, including pebble accretion, grain growth, settling and core formation, whereas Section 5 explains how the two modules are put in one code and what the initial conditions are. Sections 6 and 7 show examples of fragment evolution tracks for low opacity and pebble accretion models, respectively. In Section 8, the implications of the results obtained for TD hypothesis is given.

2 PHYSICAL MOTIVATION

2.1 Isolated planet evolution

Fig. 1 shows the evolution of an isolated Jupiter mass planet contracting from an initial state in which its central temperature is 100 K. The planet's metallicity is set to solar, and opacity is set to that of the interstellar gas/dust mix (Zhu, Hartmann & Gammie 2009). The calculation is done with the part of the code described in Section 4, although grain growth and grain sedimentation within the planet are neglected. The top panel of Fig. 1 shows the evolution of planet's radius, R_p, in units of Jupiter's radius, R_J, whereas the bottom panel shows the planet's central temperature.

The planet's evolution is conveniently described in two stages (Bodenheimer 1974). In the first 'pre-collapse' stage, the planet's central temperature is below ∼2000 K, and hydrogen is in the molecular form. As temperature exceeds ∼2000 K, H_2 molecules begin to dissociate. The process of breaking the molecules up requires 4.5 eV per hydrogen molecule, which is very large: it is equivalent to the thermal kinetic energy of two H atoms at temperature $T \approx 10^4$ K. The dissociation process is therefore a huge energy sink, and leads to the planet losing its hydrostatic equilibrium and collapsing dynamically. The new, post-collapse, equilibrium is such that H is atomic and partially ionized, central planet's temperature is well above 10^4 K, and the planet radius is more than 10 times smaller than in the pre-collapse state. In Fig. 1, the dynamical collapse corresponds to the nearly vertical part of the radius and temperature evolution curves. After the collapse, the planet arrives on the post-collapse stage, which is one and the same as the 'hottest start' track for giant gas planets (e.g. Marley et al. 2007). In Fig. 1, this post-collapse part of the evolution begins at the blue 'o' symbol in the top panel of the figure. During this phase, the planet contracts from $R_p \gtrsim 10R_J$ to $R_p \sim 2R_J$ relatively rapidly, e.g. in some 10^5 yr, and then takes much longer to eventually contract to $1R_J$.

2.2 Tidal disruption of protoplanets

The key point to observe from the top panel of Fig. 1 is just how extended the planet is at birth ($R_p \sim 1$ AU, or about $2000R_J$), and that it takes over a million years for the planet to contract to radii comparable to that of Jupiter. The red solid horizontal lines show the Hill radius, R_H, of the planet at three distances from a $M_* = 1\,M_\odot$ host star. When R_p is larger[2] when R_H, tidal forces from the star exceed self-gravity of the planet, and it can be disrupted, as in the original Kuiper (1951) scenario. Fig. 1 thus shows that the planet can be tidally disrupted at the planet–star separations $1 \lesssim a \lesssim 10$ AU in the pre-collapse stage. In addition, the planet can be tidally disrupted in the post-collapse stage in the innermost 'hot' region of the disc, $a \lesssim 0.1$ AU, provided the collapse happened very recently (no more than $\sim 10^5$ yr earlier). Nayakshin (2011a) and Nayakshin & Lodato (2012) proposed that such hot disruptions may be the origin of 'hot' sub-giant planets such as hot super-Earths or hot Neptunes.

The astrophysical metal components of the protoplanet (that is, all elements heavier than H and He) can settle into the centre of it provided that condensation temperature of the components is higher than the central temperature of the planet. In this paper, we limit our attention to three dominant grain species: water ice, organics called CHON, and a mix of Fe and silicates (cf. Section 4.3 below). The condensation temperatures for these species are marked approximately by the position of the respective text in the bottom panel of Fig. 1. Note that the planet spends little time in the cold configuration, since it cools relatively rapidly initially. From this, one can expect water to be the least able to condense down in TD planets, whereas Fe and silicates be the most able to do so (this agrees with results of Forgan & Rice 2013b, that TD cores are mainly composed of rocks).

Grain sedimentation may lead to core formation inside of the protoplanet (e.g. McCrea & Williams 1965; Boss 1997; Helled & Schubert 2008). If the gaseous component of the protoplanet is then disrupted by the tides, the nearly 'naked' core survives, since its density is much higher.

[2] This condition may be even stricter for young rotating planets, e.g. $R_p \gtrsim 0.5R_H$ may be sufficient for disruption, see Section 4.5 below.

2.3 TD model possible outcomes

Fate of a gas fragment formed in the outer disc by GI is sealed (Boley et al. 2010; Forgan & Rice 2013b) by the ratios of the various time-scales: $t_{\rm coll}$, the planet's contraction and collapse time-scale; $t_{\rm migr}$, the planet's migration time-scale and $t_{\rm sed}$, the grain growth and sedimentation time-scale. Qualitatively, there are several possibilities:

(i) If the migration time is the shortest of the three, the fragment is disrupted with nothing remaining of it.

(ii) If $t_{\rm sed} < t_{\rm migr} < t_{\rm coll}$, then grains sediment down before the planet is disrupted. There is therefore a remnant, a solid core, possibly surrounded by a post-disruption atmosphere remaining bound to the core if the latter is massive enough.

(iii) If $t_{\rm coll} < t_{\rm migr}$, then the planet collapses before it is disrupted, and survives as a gas giant planet, provided it is not disrupted in the 'hot' region or pushed all the way into the star.

(iv) If grain sedimentation time is the shortest of the three, and the core mass is significant, $M_{\rm core} \sim$ a few to 10 or more Earth masses, then the grain component can affect the whole fragment by either triggering its collapse (Nayakshin, Helled & Boley 2014) or destruction (Nayakshin & Cha 2012).

2.4 Broader connections of TD

Vorobyov & Basu (2005, 2006) found formation and a rapid inwards migration of massive self-gravitating gas clumps in their 2D simulations of protostellar discs. They argued that clump destruction episodes could be related to the FU Ori outbursts of young stars. Boley et al. (2010) were first to point out that gas clump migration, core formation and then envelope disruption may result in formation of terrestrial-like planets. Boley & Durisen (2010) noted that dynamics of solids can be important enough to change the fragmentation properties of the gravitationally unstable discs, and to affect the gas clump compositions. These in general do not therefore have to be same as that of their parent discs (Boley, Helled & Payne 2011).

Nayakshin, Cha & Bridges (2011), Vorobyov (2011) and Bridges et al. (2012) argued that the high-temperature environment inside the clumps (before they are disrupted) may provide a natural nursery for high-temperature inclusions found in chondrules of the Solar system. Nayakshin (2011a) proposed that prograde rotation of the pre-collapse gas fragments may have been imprinted on the spin directions of Earth and Mars, and yield enough angular momentum for proto-Earth to revive the fission hypothesis for the Moon formation.

Machida, Inutsuka & Matsumoto (2011) observed recurrent episodes of clump formation, destruction and protostellar outflow injections in 3D simulations of self-gravitating discs. Baruteau et al. (2011) and Michael et al. (2011) made detailed studies of planet migration in gravitationally unstable discs, finding migration times of order ∼10 000 yr. Cha & Nayakshin (2011) simulated in 3D a gravitationally unstable gas disc together with the grains that were allowed to grow, and found that grains grew most rapidly inside the clumps and indeed sedimented into the dense cores. Galvagni et al. (2012) made first 3D simulations of collapse of the rotating molecular clumps, noting the importance of the angular momentum and formation of the post-collapse circum-planetary discs.

It is important to note that planetesimals are not a pre-requisite for TD model, unlike for CA. In the context of TD, minor solids, such as asteroids, are remnants of larger solid bodies that were fragmented in collisions. Thus, Nayakshin & Cha (2012) argued that Kuiper and asteroid belts in the Solar system could be made in disruptions of molecular gas fragments in which some of the solids sedimented into the centre and got locked into a number of Ceres mass bodies. They found that after the gas clump disruption, the distribution of solid bodies naturally forms rings with sharp edges, as observed in the Solar system, and that this model does not have the 'mass budget deficit', resolving the two well-known problem of the classical models of the Kuiper belt (e.g. Morbidelli, Levison & Gomes 2008).

Nayakshin & Cha (2013) argued that gas accretion on relatively low-mass gas TD fragments ($M_{\rm p} \lesssim$ a few $M_{\rm J}$) is inefficient due to pre-heating effects from the planet on surrounding gas. These authors found that there is a dichotomy in the fate of the clumps. Low-mass clumps were found to migrate in rapidly at more or less constant mass, and eventually were destroyed by the host star's tides. Clumps more massive than $\sim 5\,M_{\rm J}$ were found to run away in the 'opposite' sense: accreting gas rapidly, they become as massive as $\sim 50\,M_{\rm J}$, open deep gaps in their protoplanetary discs, and stall at about the initial star-clump separation. This divergent evolution may explain the divergent results on the fate of the gas clumps in the literature (giant planets or brown dwarfs – see Nayakshin & Cha 2013, for references), since small changes to the disc parameters and the treatment of gas thermodynamics may shift the clumps from one of the other regime.

Tsukamoto et al. (2015) presented 3D radiative hydrodynamics (RHD) simulations of massive self-gravitating discs. Their approach is clearly preferable to all of the previous 2D studies (e.g. Zhu et al. 2012) and also the earlier 3D studies which used radiative cooling prescriptions (e.g. Cha & Nayakshin 2011). The RHD simulations could in principle directly address many of the issues needed for a quantitative TD population synthesis models, such as the initial clump mass (Forgan & Rice 2011, 2013a, e.g.), and the migration and clump accretion history. Tsukamoto et al. (2015) find that most of their clumps are as massive as $\sim 3\,M_{\rm J}$ at birth and grow rapidly in mass while migrating in. What is not clear is how general these results are with respect to changes in initial conditions, and how they depend on the dust opacity model assumed by Tsukamoto et al. (2015).

Here, and everywhere in the paper, only the simplest version of events is considered, in which the planets start out as self-gravitating gas fragments and do *not accrete* gas or planetesimals from the disc.

3 DISC EVOLUTION – PLANET MIGRATION MODULE

This section presents numerical methods with which planet migration and disc evolution are modelled in the paper. Here, the planet is treated as a point mass. The evolution of the internal planet's variables is considered in Section 4.

Using a 1D viscous disc evolution approach, Nayakshin & Lodato (2012) studied planet migration and planet mass loss for very massive ($M_{\rm p} \sim 10 M_{\rm J}$) gas planets in the 'hot' disc region, e.g. at $a \sim 0.1$ AU. Such massive gas fragments are always in the type II migration regime, when they open a deep gap in the disc (Lin & Papaloizou 1986). Nayakshin & Lodato (2012) were interested not only in the fate of the planets but also in the potential connection between giant planet disruptions and the FU Ori outbursts of young stars (Vorobyov & Basu 2006; Boley et al. 2010; Nayakshin 2011c). Therefore, the planet–disc mass exchange was followed in detail and on short time-scales (much shorter than a year) to compare them with the observed light curves and spectra of some observed FU Ori sources (e.g. Clarke et al. 2005; Eisner & Hillenbrand 2011).

The approach here follows that of Nayakshin & Lodato (2012) with a few changes. Since the fate of less massive gas planets and also that of even less massive remnants (solid cores, if the planets are disrupted) is of interest to us here, type I migration regime (no gap in the disc) is also included. Accretion luminosities of young stars, although calculated here automatically by the viscous disc evolution code, are of no direct interest. Therefore, the treatment of the planet's mass loss is simplified from that of Nayakshin & Lodato (2012): it is assumed that the planet is disrupted instantaneously if the disruption criteria are satisfied, and the mass deposition back in the disc is neglected for simplicity.

The protoplanetary disc is described by a viscous azimuthally symmetric one-dimensional time-dependent model that encapsulates the standard accretion disc solution of Shakura & Sunyaev (1973) with addition of the tidal torque of the planet on the disc. The disc surface density, $\Sigma(R)$, is evolved in this approach according to

$$\frac{\partial \Sigma}{\partial t} = \frac{3}{R}\frac{\partial}{\partial R}\left[R^{1/2}\frac{\partial}{\partial R}(R^{1/2}\nu\Sigma)\right] - \frac{1}{R}\frac{\partial}{\partial R}\left(2\Omega R^2\lambda\Sigma\right), \quad (1)$$

where $\Omega(R) = \sqrt{GM_*/R^3}$ is the Keplerian angular frequency at radius R, viscosity $\nu = \alpha_{\rm SS}c_{\rm s}H$, where $c_{\rm s}$ and H are the mid-plane sound speed and the disc height scale, $\lambda = \Lambda/(\Omega R)^2$ and Λ is the specific tidal torque from the planet. The latter is a weighted sum of the type I and the type II contributions,

$$\lambda = \lambda_{\rm I}(1 - f_{\rm II}) + \lambda_{\rm II}f_{\rm II}, \quad (2)$$

where $0 \le f_{\rm II} \le 1$ is a switch controlling whether the planet migrates in type II ($f_{\rm II} = 1$) or type I ($f_{\rm II} = 0$) regimes. Two-dimensional simulations (Crida, Morbidelli & Masset 2006) show that a deep gap in the disc is opened when parameter

$$\mathcal{P} = \frac{3H}{4R_{\rm H}} + 50\alpha_{\rm SS}\left(\frac{H}{a}\right)^2\frac{M_*}{M_{\rm p}} \lesssim 1, \quad (3)$$

where H is the disc vertical scaleheight at planet's location, a, and $\alpha_{\rm ss} < 1$ is the Shakura–Sunyaev viscosity parameter. We therefore set

$$f_{\rm II} = \min\{1, \exp[-(\mathcal{P} - 1)]\}. \quad (4)$$

The normalized specific torque for type II migration is given by the widely used expression,

$$\lambda_{\rm II} = \frac{q^2}{2}\left(\frac{a}{\Delta R}\right)^4 \quad R > a$$
$$\lambda_{\rm II} = -\frac{q^2}{2}\left(\frac{R}{\Delta R}\right)^4 \quad R < a \quad (5)$$

(Armitage & Bonnell 2002; Lodato & Clarke 2004; Alexander, Clarke & Pringle 2006), where $\Delta R = R - a$. We smooth the torque term for $R \approx a$, where it would have a singularity (see equation 5). We use the same smoothing prescription as Syer & Clarke (1995) and Lin & Papaloizou (1986), i.e. for $|\Delta R| < \max[H, R_{\rm H}]$, where H is the disc thickness and $R_{\rm H} = a(M_{\rm p}/3M_*)^{1/3}$ is the size of the Hill sphere (Roche lobe) of the planet.

As far as we are aware, there is no corresponding expression for $\lambda_{\rm I}$, perhaps partly because one usually studies type I migration in the limit where the planet's mass is small compared to the disc mass, so that the back reaction of the planet on the disc can be neglected. Our planets can be massive and yet still be in type I regime, especially in the outer self-gravitating disc (Baruteau et al. 2011), and also in the inner disc if viscosity parameter $\alpha_{\rm SS}$ is 'large' (e.g. greater than ~0.01–0.03). Furthermore, gas giant planets studied here are bright and can easily dominate the disc luminosity around their location, e.g. within the region $|R - a| < \max[H, r_{\rm H}]$ (see Nayakshin & Cha 2013). This may affect the thermodynamic disc structure near the location of the planet, yet none of the migration disc studies in the literature currently take this effect into account.

Faced with this uncertainty, we chose to use the simplest approach that appears reasonable and is to be improved in the future as details of type I migration are understood further. The total torque between the disc and the planet, $\Gamma_{\rm I}$, in a self-gravitating outer disc (Baruteau et al. 2011) is similar to the standard isothermal disc result (Bate, Bonnell & Bromm 2003), which yields type I planet migration time-scale ($t_{\rm I} \equiv -a/({\rm d}a/{\rm d}t)_{\rm I}$)

$$t_{\rm I} = \frac{M_*^2}{M_{\rm p}M_{\rm d}}\frac{H^2}{a^2}\Omega_{\rm a}^{-1}\left(1 + \frac{M_{\rm p}}{M_{\rm d}}\right), \quad (6)$$

where $M_{\rm d} = \pi\Sigma a^2$ is approximately the local disc mass, $\Omega_{\rm a}$ is the local Keplerian angular velocity and the $1 + M_{\rm p}/M_{\rm d}$ factor is introduced to account for a possibility that $M_{\rm p}/M_{\rm d} \gg 1$ for our planets, which is not the typical case for type I migrating planets (e.g. see section 2.1 in Baruteau et al. 2014). While the form of the factor $1 + M_{\rm p}/M_{\rm d}$ is debatable, we note that the main conclusions of this paper do not depend on this factor at all since the migrating planets are always much less massive than the disc while migrating most of their way in.

We assume that only the material close to the planet's location exchanges angular momentum with it, and that the strength of the interaction falls off away from the planet as

$$\lambda_{\rm I} = \lambda_{\rm I}'\exp\left[-\frac{|\Delta R|}{\Delta R_{\rm I}}\right], \quad (7)$$

where $\Delta R = R - a$, and $\Delta R_{\rm I} = H + R_{\rm H}$. $\lambda_{\rm I}'$ is found by requiring the total type I torque from the planet on the disc to equal that (with the minus sign) from the disc on the planet, that is, $M_{\rm p}(GM_*a)^{1/2}/(2t_{\rm I})$. In equation 6, $\Omega_{\rm a} = \sqrt{GM_*/a^3}$ is the local Keplerian angular velocity.

The migration rate of the planet is calculated from the conservation of the total (disc plus planet) angular momentum as in Nayakshin & Lodato (2012). Also as in Nayakshin & Lodato (2012), see their section 3.2, the vertical structure of the disc is calculated as in the standard Shakura & Sunyaev (1973) model, taking into account the irradiation from the star, which can dominate the disc heating at larger radii. The disc thermal balance equation takes into account the finite thermal disc time-scale, $(\alpha_{\rm SS}\Omega(R))^{-1}$, which determines how quickly the disc achieves thermal equilibrium if accretion rate varies suddenly. This is important in the inner disc, if the disc accretion rate is high and the thermal disc instability is triggered (Bell & Lin 1994). The disc opacity is from Zhu et al. (2009), multiplied by the ratio of the disc metallicity to the solar metallicity, $z_\odot = 0.015$.

Finally, it should be noted that in this paper only the outcome of the planet rapid inwards migration phase from the outer into the inner disc is studied, and a longer time-scale evolution of the survived fragments is not addressed. This would require a better treatment of type I migration, which currently remains controversial and model dependent especially for the more massive planets (Baruteau et al. 2014), and a disc photoevaporation term to be added to equation (1) to model late disc evolution. While this is relatively straight forward as disc dispersal by photoevaporation is believed to be reasonably well understood (Alexander et al. 2014), we wish to avoid introducing further parameters and complications to our model at this initial stage.

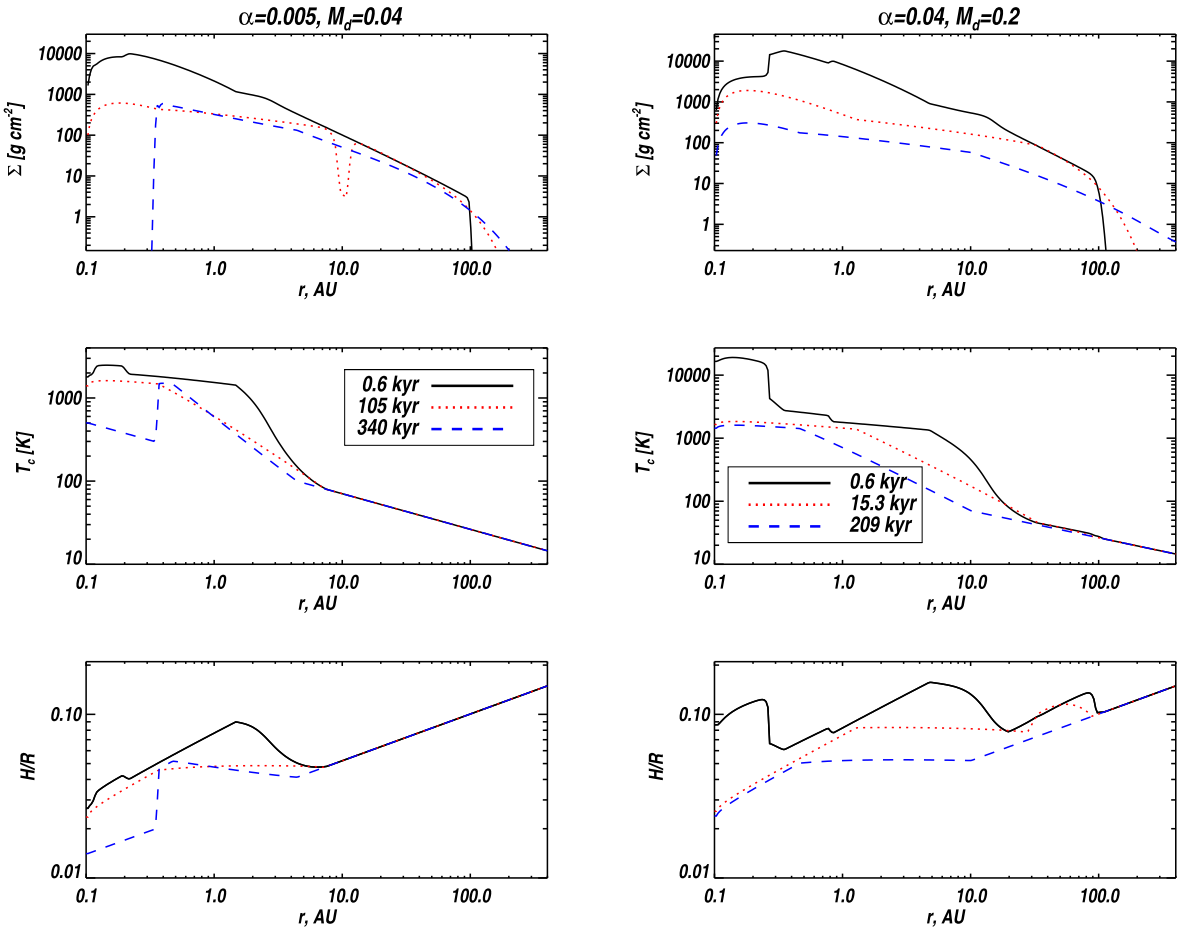

Figure 2. Disc evolution for two representative examples of a 1 M_J planet migrating in from the initial location of 75 AU. The left-hand side panels are for a low mass and viscosity disc, whereas the right-hand ones are for a high mass and viscosity disc. The panels show disc surface density, $\Sigma(R)$, the central mid-plane temperature, T_c and the geometric aspect ratio, H/R, from top to bottom, respectively. The disc profiles are shown at several times as shown in the legend.

3.1 Example disc evolution and planet migration tracks

Fig. 2 shows the disc evolution in two example calculations for a planet of a fixed $M_p = 1\,M_J$ mass migrating within a protoplanetary disc, starting from $a(t = 0) = 75$ AU. We are focused here on the migration part of the model, so we assume that the planet has already contracted to very high density and thus is not a subject to a tidal disruption. The left-hand panels of the figure show the case of a relatively low initial mass gas disc, $M_d = 0.04\,M_\odot$, and a low viscosity parameter, $\alpha_{SS} = 0.005$. The initial conditions for the disc are as described in Section 5.1, except the disc inner boundary is set to $R_{in} = 0.1$ AU in this section.

The right-hand panels of Fig. 2 contrast the low-mass disc case to a much more massive disc $M_d = 0.2\,M_\odot$ and a viscosity parameter higher by a factor of 8, $\alpha_{SS} = 0.04$. Since the steady state accretion rate in the disc scales as $\nu\Sigma$ (Shakura & Sunyaev 1973), the right-hand panels' disc produces approximately 40 times larger accretion rate on to the star than the left-hand's disc. The sub-panels of the figure show the disc surface density Σ, the central (mid-plane) disc temperature, T_c and the disc geometrical aspect ratio, H/R, at three different times as indicated in the legend. The abrupt changes in Σ and T_c of the disc in locations far away from the planet, e.g. at $R \approx 0.3$ AU, visible in the black solid curves in the right-hand panels are due to rapid dust and/or gas opacity changes at these locations.

The first disc is much cooler, so that H/R is smaller. Due to this, and since the viscosity parameter is low, the disc already develops a deep gap when the planet migrates to $a \sim 10$ AU. The gap remains deep but partially opened until the planet migrates to $R \sim 0.6$ AU, at which point the inner disc viscous time is shorter than the planet's migration time, so that the inner disc drains on to the star and there is a complete gap between the star and the planet. The planet continues to be 'pushed' inwards by the angular momentum exchange with the outer disc, and eventually perishes by going through the inner boundary of our computational domain for these tests, $R_{in} = 0.1$ AU.

In contrast, the planet is unable to open a gap of any denomination in the second test because the disc is much hotter, so H/R is higher, and because the disc viscosity is high. This planet is always embedded in its parent disc and migrates in type I regime only. The high disc viscosity in the second disc implies that this disc evolves much faster. This can be surmised from the $\Sigma(R)$ curves in Fig. 2: there is a notable decrease in the disc surface density curves at late times even at large R in the middle right-hand panel, whereas the corresponding curves on the left show that the disc evolves only inside $R \lesssim 10$ AU region for the low viscosity test.

Finally for this section, the time evolution of the disc environment around the planet in the two calculations presented in Fig. 2 is plotted in Fig. 3. Panels (a)–(c) show the planet–star separation, a, the

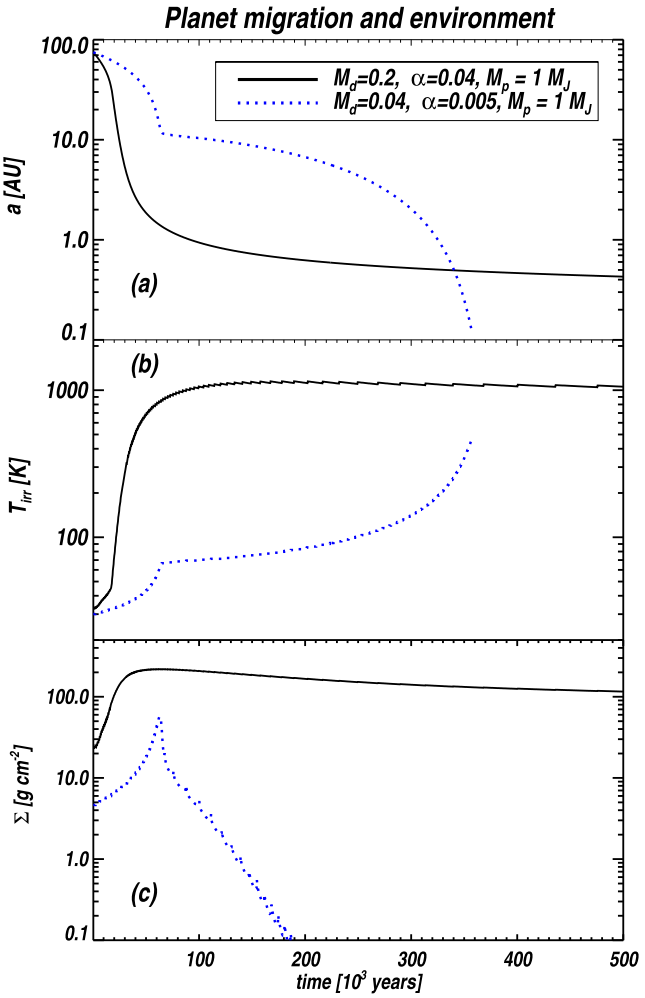

Figure 3. Planet separation versus time (panel a), irradiation temperature as seen on the surface of the planet (panel b) and the disc surface density at the location of the planet (c), for the two calculations presented in Fig. 2. Note that the hot massive disc planet (solid black curve) never opens a gap and always migrates in type I regime, whereas the other planet opens a deep gap when it reaches $a \approx 10$ AU at time $t \approx 70\,000$ yr .

irradiation temperature incident on the planet from the surrounding disc, $T_{\rm irr}$ and the disc surface density at $R = a$, respectively. The initial evolution of these quantities, from $a = 75$ AU to $a \sim 10$ AU is similar for the two planets, modulo the fact that the disc is five times less massive, and the planet migrates slower, for the blue dotted curve than for the black solid one. At smaller distances to the star, there is however a profound difference. While the hot disc planet (solid curve) continues to migrate in the type I regime, initially quickly and then slower and slower as it nears the inner disc, the other planet opens a deep gap and starts to migrate in type II regime, as we already saw in Fig. 2. Contrary to the hot disc case, the planet in the low-mass disc test accelerates as it enters the inner disc region. Therefore, somewhat contrary to intuition, the less massive and cooler disc pushes the planet through the inner boundary much faster (the hotter disc case planet arrives at the inner boundary – not shown in the figure – about a million years later).

Focusing now on the irradiation temperature evolution, two significant factors should be noted. First of all, the planet in the hotter disc is bound to find itself in hotter environment, generally. However, a secondary effect amplifies this statement manyfold: since the planet in the hot disc does not open a gap, it finds itself sampling the disc *mid-plane, e.g. central* temperature $T_{\rm c}$. The planet in the colder disc is in the gap, and that region is much cooler: the appropriate irradiation temperature is comparable to the disc effective temperature. There is a factor of at least a few difference in these two temperatures *at the same radius* R because the disc optical depth is usually considerable and hence the mid-plane temperature is higher than the effective one ($T_{\rm c} \approx T_{\rm eff}\tau^{1/4}$ in the Shakura & Sunyaev 1973 disc theory, where $\tau = \kappa\Sigma/2 \gg 1$ is the disc optical depth). In terms of irradiating flux incident on the planet, there is thus a difference by many orders of magnitude. The 'thermal bath' effect that may puff up and eventually unbind a planet (Cameron, Decampli & Bodenheimer 1982; Vazan & Helled 2012; Donnison & Williams 2014, and also Section 4.1.2 below) is therefore much stronger in the hot disc case than it is in the cold disc one.

These tests were performed for a 1 $M_{\rm J}$ planet. Gas fragments up to $\sim$10 $M_{\rm J}$ may reasonably be expected from gravitationally unstable discs (e.g. Forgan & Rice 2011). Paper III (Nayakshin & Fletcher 2015) explores the fate of gas fragments in a much broader range, from $M_{\rm p} = 0.5$ to 16 $M_{\rm J}$.

4 PLANET EVOLUTION MODULE

4.1 Radiative contraction of the planet

4.1.1 Pre-collapse evolution

Nayakshin (2010b, 2011b) and Nayakshin (2014, 2015a), employed a 1D spherically symmetric Lagrangian RHD algorithm, with grains modelled as a second fluid, to follow evolution of isolated self-gravitating gas fragments. Such a method is unfortunately too costly numerically, and lends itself to studies of only a few test cases, while we are interested in being able to investigate, eventually, thousands of models.

A more expedient 'follow the adiabats' method (e.g. Henyey, Forbes & Gould 1964; Marleau & Cumming 2014) is used in the present paper. Namely, since the energy transfer inside the planet is strongly dominated by convection at high opacities/metallicities (Helled & Bodenheimer 2011), we assume that the fragment is isentropic and is in hydrostatic balance. The initial planet is assumed to have a constant grain to total mass ratio, equal to the initial planet metallicity, z. The planet is divided into $N_{\rm b} \sim 100$ concentric equal mass gas shells with mass $\Delta M = (1 - z)M_{\rm p}/N_{\rm b}$, where $M_{\rm p}$ is the initial planet's mass. Given the central fragment's temperature, $T_{\rm c}$, at some time t, the structure of the isentropic planet can be found by iterations on the central gas density, $\rho_{\rm c}$, subject to the condition that pressure vanishes at the outer boundary. This procedure yields planetary radius, $R_{\rm p}(t)$, the total energy of the planet (gravitational plus internal), $E_{\rm tot}(t)$ and all the internal properties of the planet, e.g. the radial coordinates for all of the radial mass zones within the planet, $R(M, t)$, as a function of mass enclosed within the shell, M. In addition, the radiative luminosity, $L(M)$, is calculated. $L(M)$ is small deep inside the planet, increases outwards and reaches a maximum value close to the planet's surface. We take this maximum value to be the radiative luminosity of the planet, $L_{\rm iso}$. This is done with the understanding that the very outer regions of the planet will in reality be radiative rather than convective; however the fact that the pressure scaleheight is usually very small compared with the planet's radius means that the error in the value of planet's radius, $R_{\rm p}$, is also small.

The inner radius of the isentropic planet is given by $R_{\rm core}$, the solid core radius, as described in Section 4.4. We do not model

the internal structure of the core. The core releases $L_{\rm core}$, the core accretion luminosity, into the rest of the planet. The total energy of the planet is evolved in time according to

$$\frac{{\rm d}E_{\rm tot}}{{\rm d}t} = -L_{\rm rad} + L_{\rm core} - \frac{GM_{\rm p}\dot{M}_z}{R_{\rm p}}, \quad (8)$$

where $L_{\rm rad}$ is the radiative luminosity is the luminosity that the planet would have in isolation, $L_{\rm iso}$, *minus* that incident on the planet from the surroundings:

$$L_{\rm rad} = \max\left[0, L_{\rm iso} - L_{\rm irr}\right]. \quad (9)$$

Here $L_{\rm irr} = 4\pi\ R_{\rm p}^2\sigma_{\rm B}T_{\rm irr}^4$ is the irradiating luminosity. $T_{\rm irr}$ is equal to the surrounding disc temperature if the planet is embedded in the disc, or the local disc effective temperature if the planet opens a gap, as explained in Section 3.1. The last term on the right-hand side of equation (8) is the change in the energy of the planet if grains accrete on it at the rate $\dot{M}_z > 0$. Note that since grains accrete on the planet slowly, that is at velocities not exceeding a few m s^{-1} or else collisions would destroy the grains, the grains kinetic energy input into the planet can be safely neglected (see Sections 4.2 and 4.3, and also Nayakshin 2015b).

Note that the approach embodied by equation (9) is to separate the planet into the core and the gaseous parts and treat the two separately. We do not model the internal structure of the core in this paper, simply assuming a constant core density instead (Section 4.4). The energy released by the core as it is accreted (the $L_{\rm core}$ term) represents an energy source term for the gaseous part of the planet that we do model explicitly.

4.1.2 *The thermal bath planet disruption*

Equation (9) does not permit negative radiative luminosities for the planet for the following reasons. The structure of strongly irradiated planets, that is, when $T_{\rm irr} > T_{\rm eff}$, where $T_{\rm eff}$ is the temperature of the planet in isolation, is not isentropic since the outer layers become radiative (e.g. Burrows, Budaj & Hubeny 2008). Experimenting with strongly irradiated planets using the stellar evolution code MESA (Paxton et al. 2011), it was found that the outer layers of the planet become approximately isothermal, $T \approx T_{\rm irr}$ (see also the flat regions in T versus pressure curves in fig. 1 in Burrows et al. 2008). The radiative luminosity of the planet becomes much smaller than it is in isolation. It does not become negative, however, except for a short time required for the outer layer thermal balance re-adjustment. Furthermore, as $T_{\rm irr}$ is increased, the depth of the outer radiative layer increases. Importantly, when the layer contains a good fraction of the planet's total mass and $T_{\rm irr}$ is comparable to the planet's virial temperature, the outer layers start to expand without bounds until MESA stalls by having to use tiny time steps. Physically, the planet becomes unbound and is destroyed very quickly. This is the 'thermal bath' effect by which gaseous protoplanets are known to be destroyed when the surrounding environment is too hot (Cameron et al. 1982; Vazan & Helled 2012; Donnison & Williams 2014).

The criterion that we use to capture the thermal bath destruction of the planet is a qualitative one: we require the irradiation temperature to exceed

$$T_{\rm irr} \geq \frac{1}{2}T_{\rm vir}, \quad (10)$$

where the virial temperature of the planet is defined as $T_{\rm vir} = (1/3)GM_{\rm p}\mu/k_{\rm b}r_{\rm p}$, where $\mu = 2.4m_{\rm p}$ is the mean molecular weight.

4.1.3 *Post-collapse 'hot start' planets*

Gravitational potential of post-collapse planets is high enough to allow gas accretion on to their surface without a need for radiation since H_2 dissociation energy can be such a sink. Hence gas accretion on to the planets is much more likely in the post-collapse case than it is in the pre-collapse case (see also Nayakshin & Cha 2013). Grains, including pebbles, would accrete on to the post-collapse planet together with the gas, since such accretion would inevitably generate very hot shock fronts where pebbles would be easily vapourized and thus well mixed and coupled with the gas. However, gas accretion on to planets is not included in this paper (see Section 2) in an attempt to reduce the parameter space of the models. Therefore, our post-collapse planets do not accrete either gas or grains and hence evolve at a constant mass unless disrupted.

To model the post-collapse contraction of the planets, publically available code MESA (Paxton et al. 2011) is employed to create tables of radii, total energy and luminosity for a given mass planet for *non-irradiated* coreless giant planets at gas metallicity of $z = 0.15$. This metallicity is typical of the metallicity of the planets born in our discs due to metal loading (Nayakshin 2015a,b). The luminosity of the core is neglected in the post-collapse phase because the core's heat content is always much smaller than that of the post-collapse planets (unlike the pre-collapse planet case).

Having $R_{\rm p}(t)$ and $L_{\rm iso}(t)$ for isolated planets would be completely sufficient for our purposes of deducing whether the planet contracts more rapidly or gets tidally disrupted in the 'hot' region (see the $a = 0.05$ AU line in the top panel of Fig. 1, and also Nayakshin 2011a), were it not for irradiation of the planet by the surrounding disc or the central star. Due to that irradiation, the planet contracts slower than an isolated planet would do. To take this into account, we use an approach similar to that of the pre-collapse phase but employing the MESA tables created and with core luminosity and pebble accretion turned off, as explained above. In this approach the energy equation becomes

$$\frac{{\rm d}E_{\rm tot}}{{\rm d}t} = -L_{\rm rad}, \quad (11)$$

where $L_{\rm rad}$ is calculated as in equation (9). Now, having found an updated value of the planet's total potential energy, interpolations in the tables are employed to find the corresponding age of the planet and the new values for $R_{\rm p}(t)$ and $L_{\rm iso}(t)$. The contraction step can now be repeated, and hence $R_{\rm p}(t)$ for a migrated irradiated planet is found.

The post-collapse planets can in principle be disrupted due to either tides (Section 4.5) or the thermal bath effects (Section 4.1.2), but in the present paper none of our planets go through such disruptions.

4.2 Grain dynamics

Grain sedimentation is of course important only in the pre-collapse planets since post-collapse planets are too hot to permit existence of grains. In this paper, grains are treated as a perturbation to gas dynamics. Having found $R(M, t)$ and $R(M, t + \Delta t)$ as described in Section 4.1.1, we find the gas velocity for every mass shell in the planet,

$$u(M, t) = \frac{R(M, t + \Delta t) - R(M, t)}{\Delta t}. \quad (12)$$

If grains are sufficiently small, e.g. $a_{\rm g} \lesssim 0.01$ cm in practice, where $a_{\rm g}$ is a spherical grain's radius, then they follow the gas motion closely due to a strong aerodynamic coupling. However, in

general grain dynamics can be different from that of the gas, therefore grain sedimentation is modelled as in section 3.4 of Nayakshin (2010b). Grains are assumed to reach their terminal sedimentation velocity (with respect to gas) quickly,

$$-u_{\rm sed} = (u_{\rm a} - u) = -\frac{4\pi\, G \rho_{\rm a} a_{\rm g} R}{3 c_{\rm s}} \frac{\lambda + a_{\rm g}}{\lambda}, \quad (13)$$

where $u_{\rm a}$ is the grain velocity in the frame of the centre of the planet (which is motionless in an isolated planet case but is moving with the planet if the latter is embedded in the disc), R is the radius of the given mass shell inside the planet, $\rho_{\rm a}$ is material density of the grain, $a_{\rm g}$ is the grain size, $c_{\rm s}$ is the gas sound speed and λ is the mean free path of H_2 molecules. Equation (13) joins smoothly the Epstein and the Stokes drag regimes.

Grain sedimentation is opposed by turbulent grain mixing (e.g. Dullemond & Dominik 2005) and convection (e.g. Helled & Bodenheimer 2011). These two processes can be combined to give a diffusion coefficient, D, and be modelled as diffusion of grain concentration, $\rho_{\rm g}/\rho$ (Fromang & Papaloizou 2006). The equation describing this process is

$$\frac{\partial(\rho_{\rm g}/\rho)}{\partial t} = \frac{D}{R^2}\frac{\partial}{\partial R}\left[R^2 \frac{\partial(\rho_{\rm g}/\rho)}{\partial R}\right]. \quad (14)$$

This defines mean grain diffusion velocity, $u_{\rm diff}$,

$$u_{\rm diff} = -D\frac{\partial}{\partial R}\left[\frac{\rho_{\rm g}}{\rho}\right]. \quad (15)$$

Since the grain concentration, $\rho_{\rm g}/\rho$, is highest in the planet's centre due to grain sedimentation, the mean diffusion velocity is positive, confirming that this process opposes grain settling. The diffusion velocity is combined with the sedimentation velocity to give the total grain velocity in the planet's centre of mass frame,

$$u_{\rm a} = u - u_{\rm sed} + u_{\rm diff}. \quad (16)$$

This defines the grain mass flux in or out of the Lagrangian gas mass shells in the planet, which then defines the rate of change of the grain density $\rho_{\rm g}$ at every shell. Updating $\rho_{\rm g}$ through these mass fluxes is equivalent to solving the grain mass continuity equation,

$$\frac{\rm d}{{\rm d}t}\left[R^2\rho_{\rm g}\right] = -\frac{\rm d}{{\rm d}R}\left[R^2\rho_{\rm g}u_{\rm a}\right]. \quad (17)$$

The diffusion coefficient D takes into account two effects: turbulence and convection. For the former, a turbulence parameter $0 < \alpha_{\rm t} \ll 1$ is introduced,

$$D_{\rm turb} = \alpha_{\rm t} R_{\rm p} c_{\rm s}, \quad (18)$$

where $R_{\rm p}$ is planet's radius and $c_{\rm s}$ is the local sound speed. Convective contribution to D is (Helled & Schubert 2008) given by

$$D_{\rm conv} = l_{\rm conv} v_{\rm conv}, \quad (19)$$

where $l_{\rm conv}$ is the local gas scaleheight, and $v_{\rm conv}$ is the speed with which convective eddies rise. On the basis of the mixing length theory of convection (Kippenhahn & Weigert 1990),

$$D_{\rm conv} = \left[\frac{F_{\rm conv} g \mu l^4}{7 k_{\rm b} \rho T}\right]^{1/3}, \quad (20)$$

where $g = GM(R)/R^2$ is the local gravitational acceleration and $F_{\rm conv}$ is the local convective flux. The two contributions are added together linearly, so

$$D = D_{\rm turb} + D_{\rm conv}. \quad (21)$$

It should be emphasized that turbulence and convection are very important in opposing grain sedimentation and therefore core's growth (Helled & Schubert 2008; Helled & Bodenheimer 2011). If $u_{\rm diff}$ is sufficiently large then grains cannot sediment and in this case $\rho_{\rm g}/\rho = {\rm const}$ everywhere inside the planet to a good approximation, as we shall see later on.

The procedure just described is in place for all of the three grain species, independently of one another. This is necessary because the species have different sedimentation velocities, grain size $a_{\rm g}$, and are distributed differently inside the planet. This approach is however still a simplification of reality. The different species considered may be actually mixed in a single grain. However, since the three components we consider are well separated in their condensation temperatures (∼150, 350 and 1400 K, approximately, for water, CHON and rocks, respectively), it is not clear how poor our no-mixing approximation is. In any event, the chemistry model needs to be improved in the future.

4.3 Grain growth

Grains are expected to have a distribution of sizes, from interstellar values, $0.005\ \mu{\rm m} \lesssim a_{\rm g} \lesssim 1\ \mu{\rm m}$ (Mathis, Rumpl & Nordsieck 1977), to perhaps as large as a few cm by radius due to grain growth. A collision-fragmentation model for dust grains is necessary to follow the grain size distribution (e.g. Dullemond & Dominik 2005; Helled & Bodenheimer 2011). The grain distribution function is also a function of position inside the planet. Such a complicated treatment is well beyond our numerical resources, given that grain growth is only one of the important processes that is modelled here. In addition, physical uncertainties in grain growth and fragmentation processes would require introducing new poorly constrained parameters, greatly increasing the parameter space for the population synthesis models.

Following Nayakshin (2011b, 2014), grain growth is captured in a simpler framework. The grain distribution function over grain sizes is approximated by just two components: the 'small' and the 'large' grains. The small grains are always present due to fragmentation of larger grains in collisions, as suggested by observations and modelling of grain growth in protoplanetary discs (Dullemond & Dominik 2005). We assume that the small grains are tightly bound to gas, do not sediment, and are, of course, the dominant source of dust opacity.

The population of large grains is represented by a single size $a_{\rm g}$ and is allowed to move relatively to the gas as described above. The size $a_{\rm g}$ should be thought as a typical radius of the large grain population in a given gas mass shell. $a_{\rm g}$ varies with time due to grain growth, fragmentation, vapourization and motion of the grains from one radial cell to another. These processes are treated almost exactly as in Nayakshin (2014), and hence we only give a brief summary of what is done and point out the differences.

Large grains grow due to Brownian motion of small grains, and by sticking collisions as they sediment (cf. Boss 1998; Nayakshin 2010b):

$$\left(\frac{{\rm d}a}{{\rm d}t}\right)_{\rm grow} = \frac{\rho_{\rm g}}{4\rho_a}\left[u_{\rm Br} + u_{\rm sed} f_{\rm sb}(x)\right], \quad (22)$$

where $u_{\rm Br}$ is Brownian velocity here set to $10\ {\rm cm\ s^{-1}}$ (see section 2.4 in Nayakshin 2014), which is typically much smaller than the sedimentation velocity. The 'stick-or-break function' $f_{\rm sb}(x)$, where $x = u_{\rm sed}/u_{\rm max}$, is given by

$$f_{\rm sb}(x) = 1 - x. \quad (23)$$

This simplifies the treatment of grain collisions used in section 2.6 of Nayakshin (2014), but achieves the same physical goal:

grain–grain collisions are perfectly sticking for $u_{\rm sed} \ll u_{\rm max}$, but become fragmenting when sedimentation velocity exceeds $u_{\rm max}$ (note that $f_{\rm sb}(x > 1) < 0$). The possible grain cross-fragmentation, e.g. Fe grains fragmenting silicate grains (Nayakshin 2014), is neglected in this paper for simplicity.

The maximum velocity, $u_{\rm max}$, under which grain sticking is still possible, depends on properties of the material and is best inferred from experiment. There is however a large uncertainty here. $u_{\rm max}$ was measured to be a few m s^{-1} for both silicate (Blum & Münch 1993; Blum & Wurm 2008; Beitz et al. 2011) and icy materials (Shimaki & Arakawa 2012), but Deckers & Teiser (2013) report first laboratory experiments on decimetre-sized dust agglomerates that are bound by surface forces only (rather than by chemical bonds important for materials such as gypsum), and find $u_{\rm max}$ as small as 0.16 m s^{-1}. Pure metallic Fe grains may have $u_{\rm max}$ as large as 300 m s^{-1}, although interstellar amorphous Fe grains are probably considerably weaker (see discussion in section 2.6.1 in Nayakshin 2014). By performing numerical experiments, it was found that $u_{\rm max}$ is an important parameter of the model as it controls the maximum speed with which grains can sediment, and hence the core can be assembled. It is thus left as a free parameter of the models.

Grain vapourization rate, $({\rm d}a/{\rm d}t)_{\rm vap}$, is calculated exactly as in section 2.5 of Nayakshin (2014). Grains vapourize rapidly when the surrounding gas temperature exceeds the vapourization temperature for given species; the vapourization temperature is a function of gas pressure.

Finally, due to diffusion and sedimentation grains may enter or leave a given mass shell, which leads to a change in the grain size if $a_{\rm g}$ is different in different regions of the planet. Utilizing the grain mass conservation equation (17), we write

$$\left(\frac{{\rm d}a_{\rm g}}{{\rm d}t}\right)_{\rm adv} = -\frac{1}{r^2\rho_{\rm g}}\frac{\rm d}{{\rm d}r}\left[a_{\rm g} r^2 \rho_{\rm g} u_{\rm a}\right]. \tag{24}$$

This is an 'advective' change in the grain size. Combining all these processes, we write the full equation for grain growth as

$$\frac{{\rm d}a}{{\rm d}t} = \left(\frac{{\rm d}a}{{\rm d}t}\right)_{\rm grow} + \left(\frac{{\rm d}a}{{\rm d}t}\right)_{\rm vap} + \left(\frac{{\rm d}a_g}{{\rm d}t}\right)_{\rm adv}. \tag{25}$$

Grain abundances are as in section 2.8 of Nayakshin (2014), except silicates and Fe are combined in one refractory species. The solar abundance of metals is defined as $z_\odot = 0.015$ (Lodders 2003), which is divided amongst the grain species such that the fractional abundances, z_i of water, CHON and silicates are 0.5, 0.25, 0.25 times metallicity z, respectively. For material density of grains we use $\rho_{\rm a} = 3.5$ g cm^{-3}, 1.5 and 1.0, for silicates, CHON and water ice, respectively.

The processes of grain growth and sedimentation impose their own constraints on the maximum time step Δt, which may be more stringent than those from Section 4.1. The time step is required to be small enough that none of the grain properties change by more than 10 per cent between any two successful models of planetary structure.

4.4 Core formation and growth

The inner boundary of our computational domain is at the core's radius, $R_1 = R_{\rm core} = (3M_{\rm core}/4\pi\rho_{\rm core})^{1/3}$, where $\rho_{\rm core} = 3$ g cm^{-3}. This radius is many orders of magnitude smaller than the outer radius of the planet, $R_{\rm p}$. The structure of the planet at such small radii is unresolved in our simulations. The boundary conditions applied at $R_1 = R_{\rm core}$ is $u = 0$ and $L(R_1) = L_{\rm core}$.

As in Nayakshin (2011b, 2014), the core accretion rate depends on velocity with which grains sediment, $u_{\rm a} - u$, at the first radial zone above the inner boundary,

$$\frac{{\rm d}M_{\rm core}}{{\rm d}t} = \psi(a_{\rm g}) \begin{cases} M_{\rm d,1}(u_2 - u_{\rm a2})/R_2 & \text{if } u_2 - u_{a2} > 0 \\ 0 & \text{otherwise.} \end{cases} \tag{26}$$

Here $M_{\rm d,\,1}$ is the mass of the dust in the first gas zone, R_2 is the outer radius of the first gas zone and $(u_2 - u_{\rm a2})$ is the velocity with which grains arrive into the first zone from the second gas zone.

The function $\psi(a_{\rm g})$ is introduced to quench growth of the core in the cases where $a_{\rm g} \ll 1$ cm, when grains should be coupled to gas tightly. While the code reproduces the expectation that ${\rm d}M_{\rm core}/{\rm d}t$ is very small for small $a_{\rm g}$ (since $|u_2 - u_{\rm a2}|$ is very small), some spurious core growth at small levels does occur. To turn this unphysical growth off, the functional form of $\psi(a_{\rm g})$ is chosen to be

$$\psi(a_{\rm g}) = \exp\left[-\left(\frac{0.1\ {\rm cm}}{a_{\rm g}}\right)^2\right]. \tag{27}$$

This treatment is applied to all of the three grain species independently, to determine the accretion rate of these on to the core. These accretion rates are then added up to give the total core accretion rate. The core's mass is set to a negligibly small value in the beginning of the simulations.

Energy release by the core may have important effects on to the rest of the planet. The simplest approach would be to follow the CA prescription according to which the core luminosity is

$$L_{\rm core}^{\rm (CA)} = \frac{GM_{\rm core}\dot{M}_{\rm c}}{R_{\rm core}}, \tag{28}$$

where $\dot{M}_{\rm c}$ is the instantaneous accretion rate of the solids on to the core. However, this approach is likely to strongly overestimate $L_{\rm core}$ during its assembly *in TD framework* since this assumes that radiation diffuses out of the core rapidly. This is probably wrong as opacity of solid cores is very significant. The modelling of cooling of initially hot rocky planets above Earth mass is still very uncertain due to insufficient data on opacities, convection, conduction and other material properties at the appropriate temperature and pressure ranges (e.g. Stamenković et al. 2012). The atmospheres of such planets (the gas layers immediately adjacent to the core) could hinder rapid cooling. For example, Lupu et al. (2014) derive cooling time-scales for the atmospheres of Earth-like planets to be as long as 10^5–10^6 yr, whereas core assembly times in our models may be as short as $\sim 10^4$ yr.

Since a self-consistent treatment of the internal structure of the cores is well beyond the scope of our work, a parametrization of core accretion luminosity is made following Nayakshin et al. (2014), in which the core emits its accretional energy on a finite time-scale, $t_{\rm kh}$, where $t_{\rm kh}$ is the Kelvin–Helmholtz contraction time of the solid core. Specifically,

$$L_{\rm core} = \frac{E_{\rm core}}{t_{\rm kh}}, \tag{29}$$

where $E_{\rm core}$ is the residual potential energy of the core, which is integrated in time according to

$$\frac{{\rm d}E_{\rm core}}{{\rm d}t} = \frac{GM_{\rm core}\dot{M}_{\rm c}}{R_{\rm core}} - \frac{E_{\rm core}}{t_{\rm kh}}. \tag{30}$$

$M_{\rm core}$ and $R_{\rm core}$ are the running (current) core's mass and radius. Evidently, if $t_{\rm kh} = \infty$, then $E_{\rm core}$ is exactly equal to the potential energy of the core's assembly at mass $M_{\rm core}$. The core's luminosity is zero in this case. In more general case, if $t_{\rm kh} \gg M_{\rm core}/\dot{M}_{\rm c}$, then

$L_{\rm core} \ll L_{\rm core}^{\rm (CA)}$, but the total energy emitted by the core in the limit $t \rightarrow \infty$ is the same ($GM_{\rm core}/2R_{\rm core}$, where the final value of the core's mass and radius are used). In the opposite limit, when $t_{\rm kh} \ll M_{\rm core}/\dot{M}_{\rm c}$, $L_{\rm core} = L_{\rm core}^{\rm (CA)}$. In this paper, $t_{\rm kh} = 10^5$ yr for all of the runs presented. Preliminary results indicate that dependence of the results on $t_{\rm kh}$ is moderately weak unless $t_{\rm kh}$ is longer than a few million years, in which case most of the core's energy is saved 'for later', that is accumulated for release after the protoplanetary disc is removed.

4.5 Tidal destruction of the planet

We assume that the gas envelope of the gaseous giant planet is *completely* tidally disrupted when the planet fills a large fraction of its Roche lobe radius, e.g. when

$$r_{\rm p} > 0.7 r_{\rm H}. \quad (31)$$

The factor in front of $r_{\rm H}$ in this expression depends on the rotation state of the planet. If the planet is in a synchronous rotation with the star, as is usually the case for stellar binary systems (e.g. Ritter 1988), then this factor is nearly unity. For hydrodynamical simulations of planets embedded in discs, Galvagni & Mayer (2014) suggest the factor is 1/3 whereas Zhu et al. (2012) find it closer to 0.5. These simulations however sample the earliest phase in the evolution of the planets, some $\sim 10^3$ to perhaps 10^4 yr into their existence. During this early phase, the planets are most rapidly rotating due to a significant angular momentum at formation (e.g. Boley et al. 2010), hence they may be quite aspherical and hence easier to disrupt by tides. The factor of 0.7 in equation (31) is probably more relevant for the typically older planets that are studied here. Our main results do not depend on this factor sensitively.

4.6 Pebble accretion rate

Lambrechts & Johansen (2012) show that massive bodies accrete pebbles in the 'Hill regime', that is when all of the pebbles streaming past the planet within its gravitational reach – the Hill radius $R_{\rm H} = a(M_{\rm p}/3M_*)^{1/3}$ – are accreted. Therefore,

$$\dot{M}_z = 2 f_{\rm p} \Sigma_{\rm g}(a) v_{\rm H} R_{\rm H}, \quad (32)$$

where $v_{\rm H} = \Omega_{\rm a} R_{\rm H}$, $\Omega_{\rm a} = (GM_*/a^3)^{1/2}$ and $\Sigma_{\rm g} = f_{\rm g}\Sigma(R = a)$ is the grain surface density at radius $R = a$. The efficiency of accretion of large grains by the planet is a function of their size (e.g. Johansen & Lacerda 2010; Ormel & Klahr 2010), and only a fraction $f_{\rm p} < 1$ is in the pebble regime. $f_{\rm p}$ is a free parameter of the model.

Note that $\Sigma_{\rm g}(a)$ must be found self-consistently by the disc-planet interaction module (Section 3); it can vary by orders of magnitude at the same distance from the star depending on the disc time evolution, and especially on whether a gap around the planet's location is opened or not.

Having found the pebble mass accretion rate, pebbles are added to the existing population of grains in the outermost few radial zones of the planet and are then evolved in the manner described earlier.

We note that pebble accretion rate on to the fragment after its collapse is turned off. The gravitational potential well of a collapsed fragment corresponds to virial temperatures of order $\gtrsim 10^4$ K or more. This means that the fragment is surrounded by hot gas, dominated by dissociated and possibly partially ionized hydrogen. Pebbles will not be able to sediment through this gas and accrete on to the planet *separately* from the gas since even very large grains are vapourized before they reach the planet. Solids and gas are thus not separable in this regime. Gas and solids can accrete on to the planet, but would do it together. Accretion of gas on to post-collapse planets would increase their mass but would not change conclusions of this paper and therefore is not studied here.

5 COMBINING THE PLANET EVOLUTION AND THE DISC MIGRATION MODULES

The disc migration and planet evolution modules are combined together into a time-dependent code. This is relatively straight forward. The two modules are called by the main program that stores the values of all important variables at a given time step and passes the information between the two modules. In particular, the disc migration module needs to be provided with the current planetary mass, $M_{\rm p}$, which changes relatively slowly due to pebble accretion but can change abruptly due to a tidal disruption of the fragment. The planet evolution module requires the following inputs from the disc migration routine: the pebble accretion rate, $\dot{M}_z$, and the irradiation temperature, $T_{\rm irr}$. The main routine determines a time step, Δt, such that none of the planet or the disc variables change by more than a few per cent during that step. If Δt exceeds $\Delta t_{\rm max} = 10^3$ yr (a free parameter), it is set to $\Delta t_{\rm max}$.

The migration and the planet evolution modules are then executed independently from one another for the duration Δt. The exchange variables defined above are held fixed during this step. After the execution they return the information back to the main routine, which first makes a series of checks, such as a comparison of the Hill radius with the planet's radius to assess the fragment's integrity against tidal disruption, and then repeats the procedure by providing the modules with updated input parameters.

5.1 Initial conditions

The disc is initialized with the following surface density profile:

$$\Sigma_0(R) = \frac{A_{\rm m}}{R}\left(1 - \sqrt{\frac{R_{\rm in}}{R}}\right) \exp\left[-\frac{R}{R_0}\right], \quad (33)$$

where R_0 is the disc length-scale, set to $R_0 = 120$ AU. The constant $A_{\rm m}$ is calculated so that the disc contains a given initial mass $M_{\rm d} = 2\pi \int_{R_{\rm in}}^{R_{\rm out}} R{\rm d}R\,\Sigma_0(R)$. The initial surface density profile given by equation (33) is frequently used in studies of protostellar disc evolution (e.g. Matsuyama, Johnstone & Hartmann 2003; Alexander et al. 2006). The inner boundary of the disc is a free parameter, set to $R_{\rm in} = 0.3$ AU for tests in Section 6. This is done for simplicity, since a detailed study of planet evolution in the hot region $a \lesssim 0.1$ AU is beyond the scope of this paper. $R_{\rm out}$ is the outer radius of the disc radial grid, and is set to a value significantly larger than R_0.

The planet is inserted at an initial location, $a = a_0 \sim 100$ AU. The disc structure around the planet initially does not take the planet's presence into account, but this is not important in practice. The planet's mass is much smaller than the surrounding disc mass at a_0 (unless an extremely low disc mass $M_{\rm d} \sim M_{\rm p}$ is considered), and the planet is usually unable to open a gap in the disc anyway until it migrates inwards substantially, as found in 2D simulations (Baruteau et al. 2011).

The planet's initial structure is a polytropic gas sphere of a given total mass and central temperature, $T_{\rm c}$, which is a free parameter of

Table 1. Selected simulations, their parameters and main results. The columns are: $M_{\rm p}$, the initial planet mass, $M_{\rm J}$; $f_{\rm p}$, the pebble mass fraction; $f_{\rm op}$, the opacity reduction factor; $M_{\rm d}$, the initial mass of the disc, in units of $\rm M_\odot$; $\alpha_{\rm SS}$, disc viscosity parameter; $M_{\rm end}$, mass of the planet in the end of the run, in units of $M_{\rm J}$; $z_{\rm end}$, metallicity of the planet at the end of the simulation; a_* (AU), the radial location of planet disruption or collapse.

Name	$M_{\rm p}$	$f_{\rm p}$	$f_{\rm op}$	$M_{\rm d}$	$\alpha_{\rm SS}$	$M_{\rm end}$	$M_{\rm core}$	$z_{\rm end}$	a_*
M1LowOp1	1.0	0.0	1.0	0.12	0.01	0.00038	0.127	–	13.1
M1LowOp4	1.0	0.0	0.1	0.12	0.01	0.00017	0.057	–	12.6
M1LowOp7	1.0	0.0	0.01	0.12	0.01	1.0	0.045	0.015	61.1
M5LowOp1	5.0	0.0	1.0	0.12	0.01	0.00017	0.18	–	6.76
M5LowOp2	5.0	0.0	0.46	0.12	0.01	5.0	0.151	0.015	45.5
M5LowOp7	5.0	0.0	0.01	0.12	0.01	5.0	0.0	0.015	96.0
M1Peb1	1.0	0.5	1.0	0.12	0.01	1.16	2.02	0.154	48.7
M1Peb3	1.0	0.158	1.0	0.12	0.01	1.16	3.65	0.152	2.83
M1Peb4	1.0	0.089	1.0	0.12	0.01	0.0025	0.84	–	3.97

the model. The grains are initially mixed with gas uniformly, i.e. at time $t = 0$, $\rho_{\rm g}(R) = \rho(R)z_0/(1 - z_0)$, where $\rho_{\rm g}(R)$ is the total grain mass density for all of the grain species, $\rho(R)$ is the gas mass density at radius R inside the gas clump, z_0 is the initial fragment's metallicity. The volumetric density of a grain species i is given by $\rho_{{\rm g}i} = z_i\rho(R)$. For simplicity, grains have a uniform initial size $a_0 = 10\,\mu$m everywhere in the cloud.

5.2 Ending of the runs

For a giant planet to survive the formation and disc migration phase, it must stop migrating inwards at some point. This may happen on the very inner edge of the disc if the disc inner boundary is set by magnetospheric torques sufficiently far from the stellar surface. Alternatively, the disc may dissipate away due to photoevaporation (see Alexander et al. 2014, for a review) before the planet migrates all the way to the inner boundary. Clearly, the balance between the rate of the disc photoevaporation and the planet's inwards migration determines whether the planet stalls or migrates to the disc inner edge. Our type I migration model (Section 3) is too simplistic for the inner non-self-gravitating part of the disc, and therefore we do not attempt to end the simulations 'properly', that is by photoevaporating the disc (e.g. Alexander & Armitage 2009). The runs presented below are performed for just long enough for the planet to migrate from the outer disc into the inner disc, and to thus answer the more limited question of whether the giant planet-to-be survives this migration or not. While a more self-consistent ending of the simulations is needed to ascertain the eventual survival of the planets that collapsed before they migrated into the inner disc, the present study remains useful at limiting the spectrum of models that are able to overcome the tidal disruption barrier and deliver giant planets into the inner disc.

6 LOW OPACITY MODELS

This section begins presentation of different tests of the model. We begin with the case of no pebble accretion, $f_{\rm p} = 0$. The input parameters and main outcomes of selected simulations discussed in the sections to follow are summarized in Table 1. The runs are labelled as 'M1LowOpX' etc, where 'X' is an integer referring to a parameter varied within a given series of runs (see below), and the preceeding letters refer to one of the three series of runs. The number after 'M' is the initial mass of the fragment in Jupiter masses. All of the simulations are performed for the same disc parameters in this paper, the disc viscosity parameter $\alpha_{\rm SS} = 0.01$ and the initial disc mass $M_{\rm d} = 0.12\,\rm M_\odot$. The conclusions of the paper are qualitatively independent of the disc parameters. The main outcome of a simulation – fragment disruption or collapse – is best inferred from the row labelled $M_{\rm end}$, which shows the planet's mass at the end of the simulation in Jupiter masses. For runs in which the planet is disrupted, $M_{\rm end}$ is the mass of the solid core assembled inside the fragment before it was disrupted, and it is of course much less massive than the starting mass of the planet.

As we have seen in Section 2, the main challenge to forming giant planets via TD is a long contraction time of giant planets, $\sim$1 Myr for $M_{\rm p} = 1\,M_{\rm J}$, which implies that planets migrate inwards more rapidly than they contract and hence they are disrupted (see also Zhu et al. 2012; Vazan & Helled 2012; Nayakshin 2015a). The migration time is found to be $\sim 10^4$–10^5 yr, depending on disc parameters and the planet's mass (e.g. Boley et al. 2010; Cha & Nayakshin 2011; Baruteau et al. 2011).

In order to get more giant planets to survive the fast inwards migration, the radiative contraction time of the planets is to be shortened somehow. One way of achieving this is to invoke grain growth and therefore dust opacity reduction (e.g. Helled & Bodenheimer 2011; Mordasini 2014). To test this possibility, a series of tests in which the opacity of Zhu et al. (2009) is multiplied by arbitrary constant factors $f_{\rm op} = 10^{-(X-1)/3}$, where $X = 1, 2, \ldots 9$, is ran. Jumping ahead, for $M_{\rm p} = 1\,M_{\rm J}$, it is found that opacity reduction of around 100 is needed for the planet to survive.

6.1 Low-mass fragments

Fig. 4 shows the simulation M1LowOp4 with $f_{\rm op} = 0.1$ ($X = 4$). The upper panel (a) presents the evolution of the planet's location, a, planet's radius, $R_{\rm p}$, and the Hill radius, $R_{\rm H}$, with the solid, dotted and dashed lines, respectively. The planet starts off at $a = 100$ AU and migrates inwards on the time-scale of $\sim$20 000 yr. Initially, the planet is much more compact than the Hill radius, but $R_{\rm H}$ shrinks as the planet's orbit shrinks whereas the planet's radius does not. This eventually causes planet's disruption at $t \approx 30\,000$ yr.

The middle panel (b) of the figure shows several temperature characteristics of the planet. In particular, the blue dash–dotted line shows the effective temperature of the planet in isolation, $T_{\rm iso}$, that is defined by $L_{\rm iso} = 4\pi R_{\rm p}^2\sigma_{\rm B}T_{\rm iso}^4$, where $L_{\rm iso}$ is the isolated planet luminosity (cf. equation 9). The dotted red curve shows the irradiation temperature. Since $T_{\rm irr} > T_{\rm iso}$ already at birth of the planet, the planet cannot contract radiatively, since $L_{\rm rad} = 0$ according to equation (10). For this reason, the planet does not contract; $T_{\rm c} = {\rm const}$ and $R_{\rm p} = {\rm const}$.

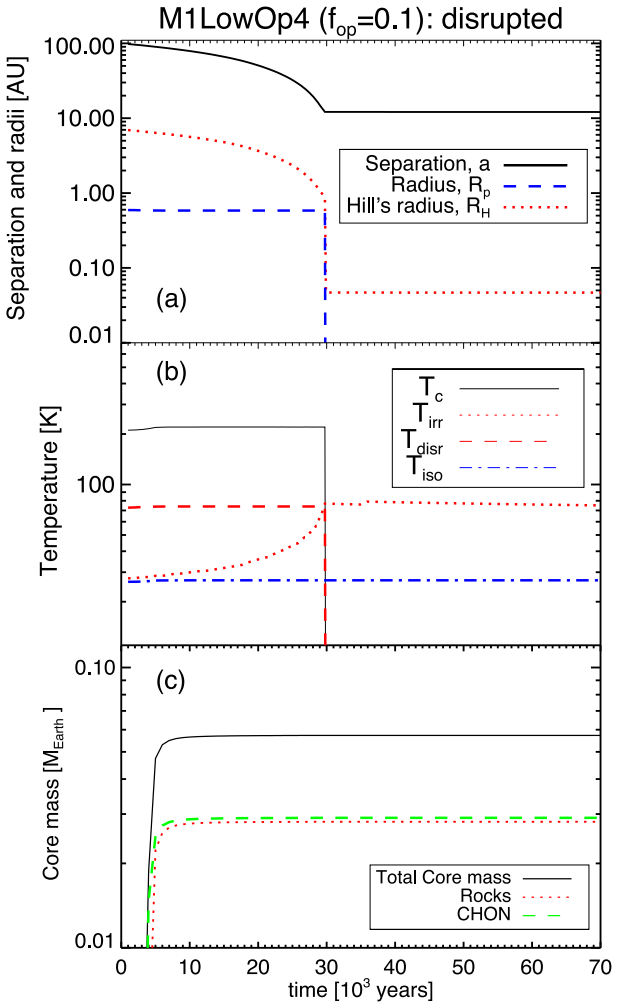

Figure 4. Simulation M1LowOp4 (see Table 1). 'Thermal bath disruption' of an $M_{\rm p} = 1\,M_{\rm J}$ planet migrating from its birth location at $a = 110$ AU occurs at $t \approx 30\,000$ yr. Panel (a) shows disc-planet separation, planet radius and the planet's Hill radius, as detailed in the legend. Panel (b) shows central temperature of the planet, $T_{\rm c}$, irradiating, disruption and the effective temperature that the planet would have in isolation. Panel (c) shows the total core mass (solid curve) and how it breaks by the composition, as labelled in the legend.

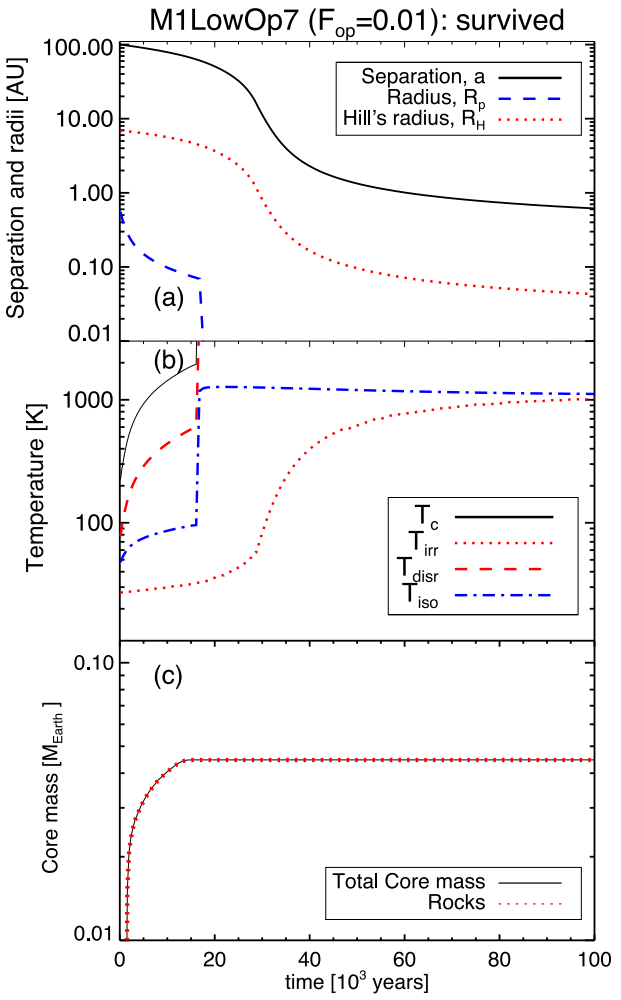

Figure 5. Same as Fig. 4 but for run M1LowOp7 (planet's opacity set to $f_{\rm op} = 0.01$). The planet radiative contraction is now faster than before and hence it is able to collapse before it is tidally disrupted.

Since the planet continues to migrate inwards rapidly, it is eventually destroyed. As is seen in panel (b) of Fig. 4, $T_{\rm irr}$ increases rapidly as the planet migrates in, and at $t = 30\,000$ yr the thermal bath planet destruction (Section 4.1.2) takes place since $T_{\rm irr}$ exceeds $T_{\rm disr}$. In passing, it should be noted that if the thermal bath destruction did not occur, this particular planet would have been destroyed very soon nevertheless by tidal disruption since the tidal disruption criterion (equation 31) is almost satisfied at $t = 30\,000$ yr.

Panel (c) of Fig. 4 shows the mass of the solid core assembled in the centre of the protoplanet. The remnant of the disruption is a low-mass solid core, $M_{\rm core} = 0.057\,{\rm M}_{\oplus}$. It is composed almost equally of CHON and silicates. The presence of CHON materials in the core is explained by the arrested evolution of the planet: since it is unable to cool and contract, it stays relatively cold for longer, and this enables CHON grains to sediment down into the core. Water ice cannot condense out even in these conditions, which is consistent with earlier results of Forgan & Rice (2013b) who found that TD cores contain little water.

The remnant core is very low mass, so that it does not migrate appreciably during the simulation, stalling at $a \approx 12$ AU. The simulations M1LowOpX were all stopped at 0.3 Myr, but the remnant's migration time is $\sim 10^7$ yr at the end of the run, so not much migration would occur in the typical 3 Myr disc lifetime even if the simulations were continued for longer.

Fig. 5 shows an identical run but with opacity further reduced, $f_{\rm op} = 0.01$, labelled M1LowOp7 in Table 1. In this case, the planet's intrinsic luminosity exceeds the irradiating one at early times (cf. the dash–dotted blue and the dotted red curves in panel b). The planet thus contracts rapidly, and its central temperature increases rapidly (the solid black curve in panel b). The planet undergoes the second collapse at $t \approx 20\,000$ yr, well before it is challenged thermally (due to external irradiation) or tidally (due to tidal forces from the star). The core of the planet is slightly less massive than in LowOp1, and is completely dominated by silicates because the planet heats up quickly and the CHON grains have little chance to sediment into the core.

Although we do not present the run M1LowOp6, for which $f_{\rm op} \approx 0.022$, we note that it ended with the planet disrupted. The conclusion from this series of tests is that opacity reduction by a factor of $\sim$100, compared to the interstellar grain opacity at solar metallicity, is needed to counter the short inwards migration times

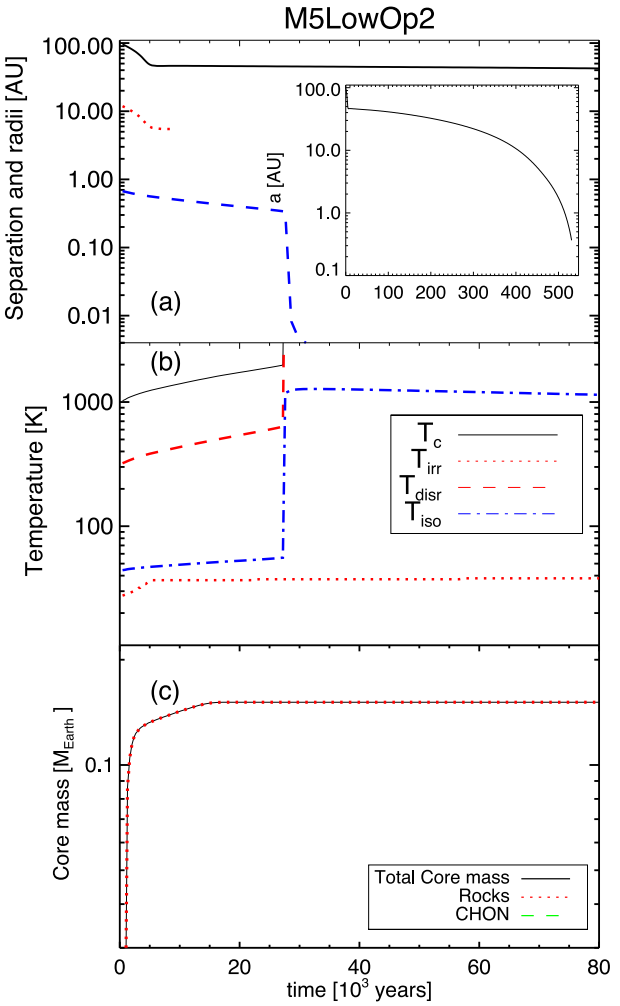

Figure 6. Same as Fig. 4 but for simulation M5LowOp2, e.g. a more massive gas fragment, $M_p = 5\,M_J$, and higher dust opacities ($f_{op} = 0.46$). The inset in panel (a) shows the longer term evolution of the planet's separation.

and the thermal bath effect, at least for the parameters of the disc and the planet mass chosen in this section.

Fig. 10 shows the mass of the cores formed in the series of runs M1LowOpX as a function of the opacity reduction factor f_{op}, and Section 8 considers broader implications of these runs for TD theory of planet formation.

6.2 Higher mass fragments

Finally for this section, Fig. 6 shows simulation M5LowOp2, where the fragment is more massive, $M_p = 5\,M_J$. The practical interest in considering more massive fragments is that such fragments cool much more rapidly than ∼ Jupiter mass ones (see fig. 1 in Nayakshin 2015a). Therefore, one may reason that dust opacity may not need to be reduced by orders of magnitude for such fragments.

Indeed, in simulation M5LowOp2 (see Table 1), $f_{op} = 0.46$, that is, the dust opacity is reduced by only a factor of 2, yet the planet is able to contract and collapse before being tidally disrupted. The collapse occurs at $t \approx 27\,000$ yr, when the planet is at separation $a \sim 46$ AU. One reason for the fast contraction of the planet is that the planet's effective isolated temperature, T_{iso}, is always above the irradiation temperature (cf. panel b), and the second is that the planet's migration is dramatically slowed down when the planet opens a gap in the disc at $a \sim 45$ AU. However, the planet eventually migrates all the way to the inner boundary condition at $R = 0.3$ AU after about 0.5 Myr (see the inset in panel a of the figure). It would become either a hot Jupiter, if its migration stalls in the regions closer to the star that are not simulated here, or be swallowed by the star completely.

Note also that despite having five times more mass in metals than the $M_p = 1\,M_J$ runs, the fragment only manages to assemble a tiny silicate core, $M_c = 0.15\,M_\oplus$ (cf. panel c of the figure and the table). This is because the fragment spends too little time in the molecular H regime (the pre-collapse stage), so that even the silicate grains have too short a time window in which to grow and sediment. This finding is consistent with results of Helled & Schubert (2008) and Helled, Podolak & Kovetz (2008) who found that the higher the mass of the fragment, the less efficient is core formation.

To save space, the simulation M5LowOp1 is not shown in figures but its results are listed in Table 1. In this higher opacity, $f_{op} = 1$ case, the planet does not manage to contract into the giant planet and is disrupted at $a = 6.7$ AU. The core formed in this simulation is only slightly more massive, $M_{core} = 0.18\,M_\oplus$.

From the M5LowOpX series of runs we learn that (i) the planet must be more massive than about 5–6 M_J to contract faster than migrate in at solar metallicity, at least for the disc parameters chosen in this series of runs, and that (ii) massive planets do not make much more massive cores than less massive planets do. This last finding is not new at all (Helled et al. 2008).

7 PEBBLE ACCRETION MODELS

7.1 Giant planet survival

In this section, models with pebble accretion on to the gas fragments and with interstellar dust opacity, scaled to the instantaneous metallicity of the fragment, are considered. The initial conditions for the disc and the planet are exactly the same as for the runs M1LowOpX, but here the opacity reduction factor is $f_{op} = 1$. Additionally, since the metallicity of the fragments now varies with time as pebbles accrete on to the fragments, the opacity coefficient is chosen to be proportional to the fragment's metallicity: $\kappa = \kappa_0(\rho, T)(z/z_\odot)$, where κ_0 is the interpolated table dust and gas opacity at solar metallicity from Zhu et al. (2009). Pebble accretion rate is calculated as described in Section 4.6.

Table 1 lists input parameters and key results from several runs of this series, which are labelled M1PebX, where X is an integer between 1 and 9 which sets the pebble mass fraction in the disc, $f_p = 0.5 \times 10^{-(X-1)/4}$. Presumably, higher metallicity discs would have higher f_{op} as grain growth is faster at higher metallicities, so high (low) values of f_{op} may be taken as a proxy for high (low) values of disc metallicity.

Fig. 7 shows the results of the run M1Peb4, $f_p = 0.089$ in the format similar to Figs 5 and 6, except that the bottom panel (c) also shows the evolution of the planet's metallicity, z, defined as the ratio of the mass of the metals to the total mass of the planet. z is shown with the cyan triple-dot–dashed curve, and the relevant scale is given on the right-hand side edge of panel (c).

Due to pebble accretion, the planet's metallicity increases with time sharply until time $t \approx 30\,000$ yr. At that point accretion of pebbles slows down since the planet starts opening a gap in the disc around its location, so that $\Sigma_g(a)$ plummets. As a result, the planet contraction slows down (note that the dashed blue curve in panel a flattens at that point). Due to a continuing inwards migration, the Hill radius of the planet (red dotted curve in panel a) continues to

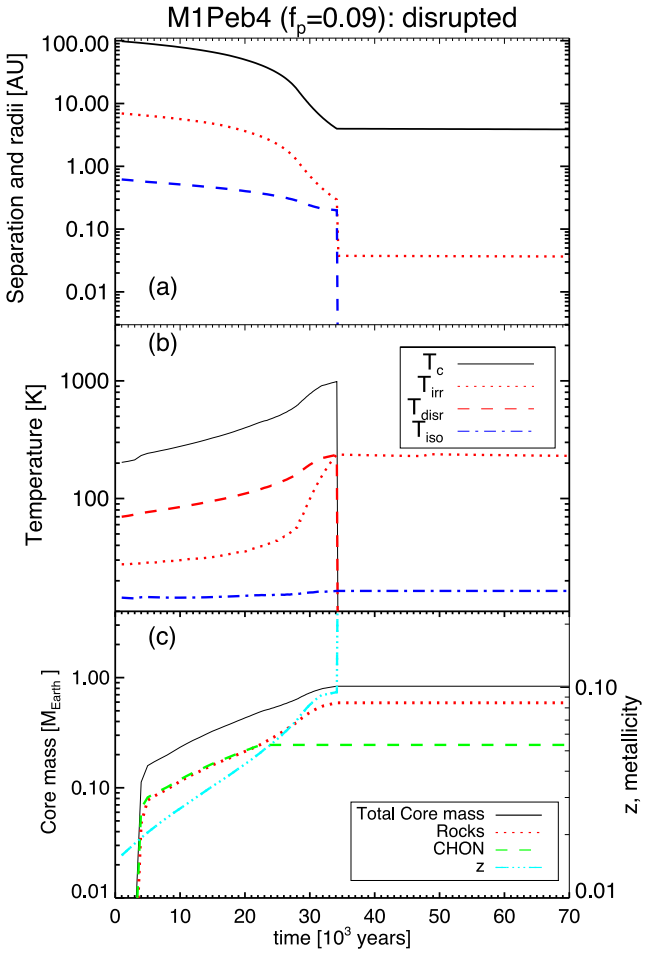

Figure 7. Same as Fig. 5 but assuming interstellar dust opacity ($f_{op} = 1$) and allowing for pebble accretion with pebble fraction in the disc $f_p = 0.09$ (run M1Peb4 in Table 1). This experiment ends in giant planet destruction and a remnant of 0.84 $M_\oplus$ masses.

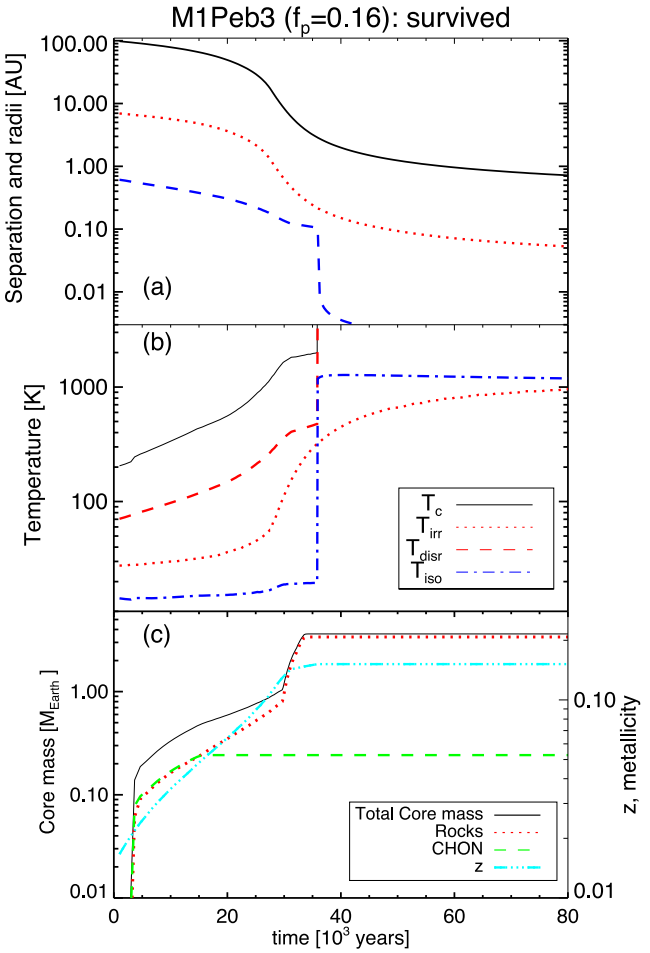

Figure 8. Same as Fig. 7 but a higher pebble fraction, $f_p = 0.16$ (M1Peb3 in Table 1). Unlike M1Peb4, the giant planet manages to contract and collapse in this case. The end result is a metal-rich, $z = 0.15$, hot Jupiter with a core mass of 3.65 $M_\oplus$.

shrink, and the planet is tidally disrupted at time $t = 34\,000$ yr, when the tidal disruption criterion (equation 31) is met.

The core's mass at that point is $M_{core} = 0.84\,M_\oplus$ and the planet's location is $a = 3.97$ AU. Since the core's possible atmosphere is neglected in this paper, the mass of the planet after the disruption is set to that of the core, and the metallicity is set to $z = 1$ by definition. Also, the temperature of the planet is arbitrarily set to 0 to make the cases of envelope disruption visibly distinct from the cases when the envelope collapses and heats up (e.g. Fig. 6). In reality, the core's temperature may be quite high but that is not modelled here (Section 4.4). The core's composition in run M1Peb4 is dominated by silicates (see panel c of Fig. 7), yet over a third of the core's mass comes from organics (CHON).

Next figure, Fig. 8, shows simulation M1Peb3, which has a slightly higher fraction of pebbles in the disc, $f_p = 0.16$. This turns out to be sufficiently high to enforce collapse of the fragment before it is tidally or thermally disrupted. Metallicity of this planet at collapse is $z = 0.152$. This higher metallicity translates into larger grain sizes in the planet (since $(da/dt)_{grow}$ term in equation 25 is larger) and a higher grain growth rate of the core. The mass of the core at collapse is $M_{core} = 3.65\,M_\oplus$. It is interesting to note that the CHON mass of the core is actually slightly lower than in the run M1Peb4, and hence the core is over 90 per cent silicates. This result is driven by a faster contraction rate of the planet in M1Peb3. The time window for CHON grains settling into the core is now shorter, so despite more CHON mass inside the planet, a smaller mass of that reservoir arrives at and is locked into the core. The planet in simulation M1Peb3 continues to migrate in a regime intermediate between type I and II regimes and eventually arrives at the disc's inner edge. The planet may survive as a hot Jupiter if the disc is removed while the planet is still migrating in or if the inner boundary of the disc is cut off by magnetospheric interactions sufficiently far from the star's surface.

Finally, Table 1 lists the results of the most pebble-rich run of the series, M1Peb1, $f_p = 0.5$. Interestingly, the higher abundance of pebbles did not increase the core's mass or the planet's metallicity at collapse. The latter is due to the fact that the planet collapses when it accretes enough pebbles (Nayakshin 2015a), which is independent of the rate at which the metals are added to the planet. The core's mass appears to be lower due to a shorter time span available for grain sedimentation.

In summary, runs M1PebX with $X = 1$, 2, 3 produced a giant planet that collapses before it was tidally disrupted, whereas runs with $X \geq 4$ resulted in tidal or thermal disruptions of the giant planets to be. Since a higher pebble accretion rate may be expected at higher metallicity environments, one expects a positive correlation of the giant planet detection frequency with metallicity of the host, as shown by Nayakshin (2015a).

7.2 Planet's internal structure

Fig. 9 shows the planet's internal variables as a function of the total (gas plus metals) mass enclosed in concentric shells for a planet from run M1Peb3 at time $t = 24\,450$ yr, before it is tidally disrupted. The planet's structure in the pre-collapse (or pre-disruption) stages are similar to one another, so Fig. 9 is representative of the pre-collapse TD planets structure in general.

The temperature in the planet, as expected, is maximum in the centre and falls off towards the planet's outer edge; see the solid curve in panel (a). In the same panel, the dotted red curve shows radius in units of AU as a function of the enclosed mass. The planet's outer radius is $R_p \approx 0.22$ AU. The blue dashed curve shows the local metallicity, $z(M)$, defined as the ratio of the metal's mass in the given mass shell to the total mass of that shell.

Note that the highest metallicity gas is at the centre of the planet, as may be expected if metals (grains) are able to sediment to the planet's centre. In addition, there are two somewhat sharp features in the $z(M)$ function, one at $M \approx 0.55\,M_J$, and the other near the outer edge of the planet. These two features mark two important transitions within the planet. The nature of these transitions is best inferred from the bottom panel of Fig. 9, (c), which shows the grain size for the three grain species that are considered in this paper: water, CHON and silicates. The vapourization temperatures for these species are very different (see Fig. 1).

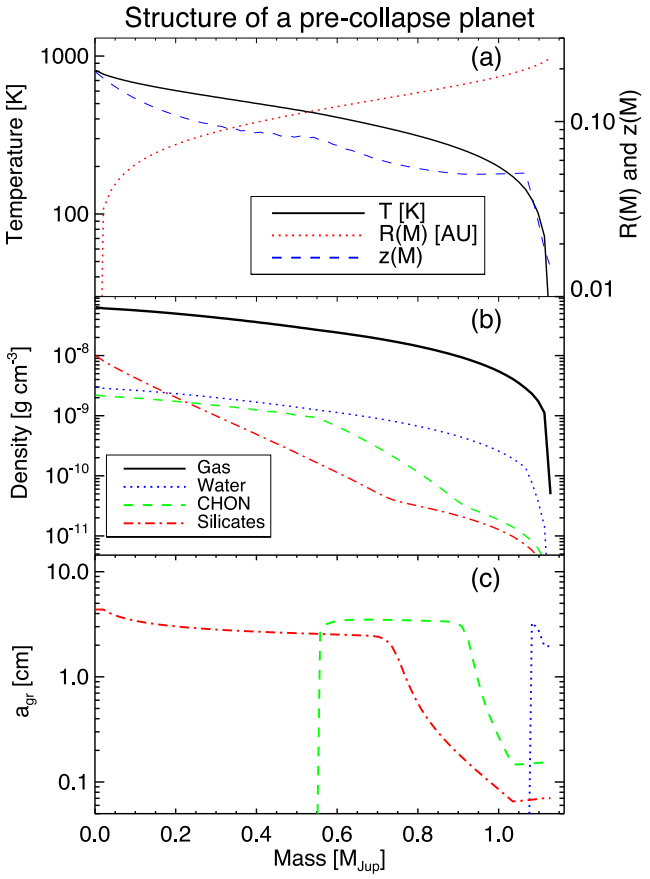

Figure 9. Internal structure of the planet at time $t = 24\,450$ yr in simulation M1Peb3 as a function of total (gas plus metals, including the core) enclosed mass. Panel (a) shows the temperature, Lagrangian radius (in units of AU) and local metallicity, $z(M)$. Panel (b) shows gas (solid) and the three grain metal species density profiles, while panel (c) shows the species' grain size, a_{gr}.

The silicate grains are the most refractory of the three, so they are able to sediment down all the way to the centre of the cloud in Fig. 9. Despite this, note that the grain size for silicates is limited to a few cm. This is a direct consequence of the grain breaking velocity set to $v_b = 10^3$ cm s^{-1} for this simulations. Larger grains would sediment faster than this and would fragment due to collisions. In the outer regions of the planet, the grains are not limited by fragmenting collisions. Instead, the limitation here comes from the balance between the rate at which the grains grow and the rate at which they sediment down: larger grains are constantly removed from the outer regions of the planet by sedimentation, so there exist a quasi-equilibrium between small growth injection at the outer edge of the cloud, grain growth and sedimentation of the grains.

Grain diffusion due to convection in particular is a very important part of this quasi-equilibrium, since convection opposes grain sedimentation (e.g. Helled & Bodenheimer 2011). Effects of convective grain mixing are best revealed by looking at the grain volume density distributions (the middle panel, b). It is notable that there are transitions in $\mathrm{d}(\rho_i/\rho)/\mathrm{d}m$, where ρ_i is the grain volume density of species i, at locations where grain size a_i changes abruptly. For example, CHON grains are 'small' in the outer region of the cloud, then 'large' between $M \approx 0.9$ and $M \approx 0.55\,M_J$, and very small again for $M \lesssim 0.55\,M_J$. Just as with silicate grains, this is because grain growth is sedimentation limited in the outer region, then fragmentation limited in the middle, and finally grain vapourization dissolves the grains and puts them into the gas phase. Convection controls CHON grains' volume distribution in the inner part of the cloud, where $\rho_{chon}/\rho = $ const to a good degree. In the fragmentation-limited range, ρ_{chon}/ρ is strongly decreasing outwards, until the grains are small and convection again takes over. Water ice grains are able to settle down only through the outermost $\sim 0.1\,M_J$ of the planet, and therefore there is a very large gradient in the water ice concentration there. In the rest of the planet water is very well mixed with the H/He phase.

These grain growth, fragmentation and convective mixing equilibria drive the chemical abundances of the species with the planet. In the outer $\sim 0.3\,M_J$ of the planet, water is more abundant than CHON and silicates by a factor of ~ 30 rather than the expected (solar) abundance ratio (two). On the other hand, silicates are over-abundant over water and CHON compared to their initial relative abundances by a factor of ~ 10 in the centre of the planet. TD fragments are hence natural thermo-mechanical element differentiation 'factories' while they are in the molecular H (pre-collapse) phase (see Nayakshin 2015a, for more on this point).

8 DISCUSSION: LOW OPACITY OR PEBBLE ACCRETION TO SAVE GIANTS IN TD?

Fig. 10 presents a bird's view of the results of the three series of runs presented in Table 1 by showing only the dependence of the core mass, M_{core}, on the pebble mass fraction, f_p, for the pebble accretion runs M1PebX (triangles), and on the opacity reduction factor, f_{op}, for the 'low opacity' runs M1LowOpX or M5LowOpX (diamonds and squares, respectively). In addition, the runs that resulted in the collapse of the giant planet rather than its disruption are connected with one another by solid segments of the same colour as the symbols. For example, the three black triangles in the upper right of Fig. 10 show the runs M1Peb1 to M1Peb3, for which the pebble mass fraction is the highest. The rest of the black triangles refer to runs M1Peb4 to M1Peb9, for which the fragments were disrupted before they could collapse.

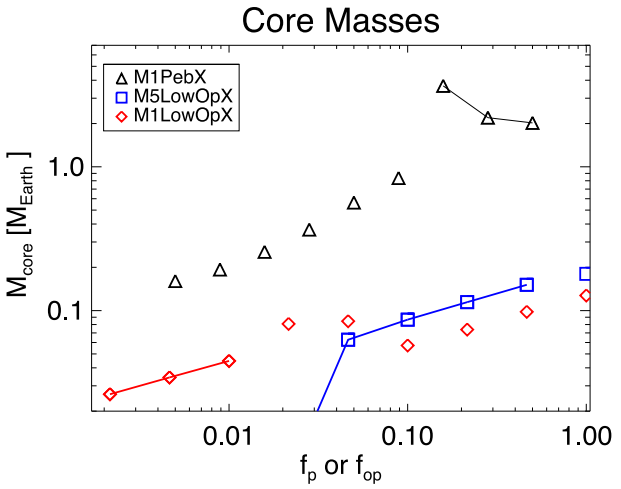

Figure 10. Core masses as a function of opacity reduction factor $f_{\rm op}$ or pebble fraction $f_{\rm p}$ for the three sets of models summarized in Table 1. The runs for which gas fragments collapsed faster than they migrated in are connected with lines. For symbols not connected with lines, the fragments were tidally disrupted and their cores released back in the disc.

It is of course expected that $f_{\rm p}$ and $f_{\rm op}$ are proportional to disc metallicity, since both are expected to increase as z increases, with other parameters being equal.

We see that opacity reduction by a factor of $\sim$100 compared to the interstellar opacity at solar metallicity is needed for planets of 1 $M_{\rm J}$ (red diamonds) to collapse sooner than they are disrupted. It could be argued that planet migration inside lower mass discs than $M_{\rm d} = 0.12\,{\rm M}_{\odot}$ used universally for all the tests in Table 1 could allow for a smaller reduction in opacity (that is, higher $f_{\rm op}$), but much lower mass discs are unlikely to become self-gravitating and give birth to a GI fragment in the first place.

Furthermore, observed giant planets in the Solar system and beyond (e.g. Miller & Fortney 2011) are known to be overabundant in metals by a factor of $\sim$10 or more than $z_{\odot}$. Thus, the needed opacity reduction is a factor of $\sim 10^3$ for the observed metal-rich giant planets of about 1 $M_{\rm J}$. While grain growth can reduce opacity (Helled & Bodenheimer 2011; Mordasini 2014), grain fragmentation should be included in such models as well (Dullemond & Dominik 2005). We have seen that collisions with grains as large as a few cm in size are frequent enough inside the pre-collapse fragments (see Section 7.2) to limit grain size by fragmentation. This was found for the breaking velocity set to $v_{\rm br} = 10\ {\rm m\ s^{-1}}$, a relatively high value, but perhaps reasonable for the refractory grains strengthened by sintering in the high-temperature environment inside the fragment (e.g. Nayakshin 2015a). Amorphous grain aggregates are found to fragment at velocities as little as $\sim 0.16\,{\rm m\,s^{-1}}$. Despite these uncertainties in the input grain physics, it is hard to imagine that fragmentation of smaller grains would not be efficient inside the pre-collapse planets. It appears unreasonable to us to require the dust opacity to be reduced by such a huge factor as $\sim 10^3$.

Even if nature does manage to reduce dust opacity to such tiny values somehow, the trends of the low opacity TD models for giant planet formation directly contradict the observations. It is obvious from Fig. 10 that low-metallicity environments would be more hospitable to planet formation via GI/TD models *if* radiative cooling was the bottle neck for giant planet contraction, in agreement with the results of Helled & Bodenheimer (2011). This trend is exactly opposite to what is observed (Fischer & Valenti 2005).

Furthermore, as seen from Fig. 10, the core masses assembled by such rapidly collapsing gas fragments would be rather small, $M_{\rm core} \sim 0.1\,{\rm M}_{\oplus}$. When the 'low opacity' run fragments (diamonds in Fig. 10) are tidally or thermally disrupted, the mass of their cores is far too small to explain rocky terrestrial planets, save for the more massive super-Earth planets.

Considering more massive gas fragments relaxes the requirement for the low opacity, as is seen from the sequence of squares in Fig. 10. For $M_{\rm p} = 5\,M_{\rm J}$, the required reduction in opacity is only a factor of $\sim$2, which is quite reasonable. However, the mass of the cores assembled inside such high-mass planets is still very low. This is because more massive planets are hotter to begin with and contract more rapidly, leaving too little time for grains to settle down (as was found previously by Helled et al. 2008; Nayakshin 2011b). Disruptions of high-mass fragments would therefore fail to explain the abundant massive rocky planets (e.g. Petigura, Marcy & Howard 2013). The high-mass gas fragments would also not be able to explain formation of lower mass giant planets, $M_{\rm p} \lesssim 1$–$2\,M_{\rm J}$, which are much more abundant in the data than planets of mass $M_{\rm p} \gtrsim 5\,M_{\rm J}$. There is also no clear reason why the high-mass radiatively cooling fragments would follow a positive metallicity correlation.

Finally, whatever the mass of the gas fragment, the low opacity models do not provide an explanation for why giant planets are found to be much more abundant in metals than their host stars.

Therefore, it is our opinion that in terms of development of TD planet formation theory that could account for all types of observed planets, low dust opacity models are not only physically unlikely, they are a dead end.

In contrast, pebble accretion models (i) yield a positive planet-metallicity correlation Nayakshin (2015a); (ii) are very metal rich, e.g. $z \gtrsim 0.1$–0.2 (cf. entry $z_{\rm end}$ in Table 1); (iii) can assemble sufficiently massive solid cores (cf. Fig. 10) to potentially explain rocky planets as remnants of disrupted gas fragments (Boley et al. 2010).

One caveat in our results is the assumption that gas does not accrete on to pre-collapse gas planets (e.g. Section 4.1.3). While plausible, this should be studied with 3D simulations of fragment-disc dynamics further.

9 CONCLUSIONS

In this article, steps are taken towards a numerically efficient way of computing the planet–disc coevolution in the framework of the TD hypothesis for planet formation. Two ways of avoiding tidal disruption during planet migration from the outer $\sim$100 AU disc into the inner one are considered: low dust opacity in the fragments and pebble accretion on to the fragments. The former pathway requires extreme dust opacity reduction (by $\sim$3 orders of magnitude), predicts a negative correlation of giant planet frequency of occurrence with metallicity, and leaves low-mass $M_{\rm core} \sim 0.1\,{\rm M}_{\oplus}$ solid cores as disruption remnants. The significant overabundance of observed giant planets in metals (Miller & Fortney 2011) is also not addressed by this class of models. Metal overabundance at birth (Boley et al. 2011) could in principle produce pre-collapse fragments that are metal rich but are low opacity, especially if grains grow quickly. Such fragments may leave massive solid cores behind when disrupted. However, such a model would still follow a negative metallicity correlation, as shown by Helled & Bodenheimer (2011).

Therefore, fragments cooling and contracting radiatively rather than due to pebble accretion are not likely to explain observed planets. The most probable physical reason for this irrelevance of

low opacity models is that collisional grain fragmentation keeps the supply levels of small grains sufficiently high (as argued for protoplanetary discs by Dullemond & Dominik 2005), so that dust opacities never drop by orders of magnitude below the interstellar values.

In contrast, high opacity ($f_{\rm op} \sim 1$) pebble accreting fragments produce a positive metallicity correlation, yield massive solid cores as remnants and also explain why giant gas planets are strongly overabundant in metals. On the basis of this paper, pebble accretion appears a key ingredient to a successful TD model for planet formation.

ACKNOWLEDGEMENTS

Theoretical astrophysics research in Leicester is supported by an STFC grant. The author thanks Richard Alexander, discussions with whom were very influential in shaping the disc evolution model of the paper. This paper used the DiRAC Complexity system, operated by the University of Leicester, which forms part of the STFC DiRAC HPC Facility (www.dirac.ac.uk). This equipment is funded by a BIS National E-Infrastructure capital grant ST/K000373/1 and DiRAC Operations grant ST/K0003259/1. DiRAC is part of the UK National E-Infrastructure.

REFERENCES

Alexander R. D., Armitage P. J., 2009, ApJ, 704, 989
Alexander R. D., Clarke C. J., Pringle J. E., 2006, MNRAS, 369, 229
Alexander R., Pascucci I., Andrews S., Armitage P., Cieza L., 2014, Protostars and Planets VI. Univ. Arizona Press, Tucson, p. 475
Alibert Y., Mordasini C., Benz W., Winisdoerffer C., 2005, A&A, 434, 343
Armitage P. J., Bonnell I. A., 2002, MNRAS, 330, L11
Baruteau C., Meru F., Paardekooper S.-J., 2011, MNRAS, 416, 1971
Baruteau C. et al., 2014, Protostars and Planets VI. Univ. Arizona Press, Tucson, p. 667
Bate M. R., Bonnell I. A., Bromm V., 2003, MNRAS, 339, 577
Beitz E., Güttler C., Blum J., Meisner T., Teiser J., Wurm G., 2011, ApJ, 736, 34
Bell K. R., Lin D. N. C., 1994, ApJ, 427, 987
Blum J., Münch M., 1993, Icarus, 106, 151
Blum J., Wurm G., 2008, ARA&A, 46, 21
Bodenheimer P., 1974, Icarus, 23, 319
Boley A. C., Durisen R. H., 2010, ApJ, 724, 618
Boley A. C., Hayfield T., Mayer L., Durisen R. H., 2010, Icarus, 207, 509
Boley A. C., Helled R., Payne M. J., 2011, ApJ, 735, 30
Boss A. P., 1997, Science, 276, 1836
Boss A. P., 1998, ApJ, 503, 923
Bowler B. P., Liu M. C., Shkolnik E. L., Tamura M., 2015, ApJS, 216, 7
Bridges J. C., Changela H. G., Nayakshin S., Starkey N. A., Franchi I. A., 2012, Earth Planet. Sci. Lett., 341, 186
Burrows A., Budaj J., Hubeny I., 2008, ApJ, 678, 1436
Cameron A. G. W., 1978, Moon Planets, 18, 5
Cameron A. G. W., Decampli W. M., Bodenheimer P., 1982, Icarus, 49, 298
Cha S.-H., Nayakshin S., 2011, MNRAS, 415, 3319
Clarke C., Lodato G., Melnikov S. Y., Ibrahimov M. A., 2005, MNRAS, 361, 942
Crida A., Morbidelli A., Masset F., 2006, Icarus, 181, 587
Deckers J., Teiser J., 2013, preprint (arXiv e-prints)
Donnison J. R., Williams I. P., 2014, Planet. Space Sci., 97, 43
Dullemond C. P., Dominik C., 2005, A&A, 434, 971
Eisner J. A., Hillenbrand L. A., 2011, preprint (arXiv e-prints)
Fischer D. A., Valenti J., 2005, ApJ, 622, 1102
Forgan D., Rice K., 2011, MNRAS, 417, 1928
Forgan D., Rice K., 2013a, MNRAS, 430, 2082
Forgan D., Rice K., 2013b, MNRAS, 432, 3168
Fromang S., Papaloizou J., 2006, A&A, 452, 751
Galvagni M., Mayer L., 2014, MNRAS, 437, 2909
Galvagni M., Hayfield T., Boley A., Mayer L., Roškar R., Saha P., 2012, MNRAS, 427, 1725
Gammie C. F., 2001, ApJ, 553, 174
Goldreich P., Tremaine S., 1980, ApJ, 241, 425
Gonzalez G., 1999, MNRAS, 308, 447
Helled R., Bodenheimer P., 2011, Icarus, 211, 939
Helled R., Schubert G., 2008, Icarus, 198, 156
Helled R., Podolak M., Kovetz A., 2008, Icarus, 195, 863
Helled R. M. et al., 2014, Protostars and Planets VI, 643
Henyey L. G., Forbes J. E., Gould N. L., 1964, ApJ, 139, 306
Ida S., Lin D. N. C., 2004, ApJ, 616, 567
Ida S., Lin D. N. C., 2008, ApJ, 685, 584
Johansen A., Lacerda P., 2010, MNRAS, 404, 475
Johansen A., Blum J., Tanaka H., Ormel C., Bizzarro M., Rickman H., 2014, Protostars and Planets VI. Univ. Arizona Press, Tucson, p. 547
Kippenhahn R., Weigert A., 1990, Stellar Structure and Evolution. Springer-Verlag, Berlin
Kuiper G. P., 1951, in Hynek J. A., ed., 50th Anniversary of the Yerkes Observatory and Half a Century of Progress in Astrophysics, p. 357
Lambrechts M., Johansen A., 2012, A&A, 544, A32
Lambrechts M., Johansen A., 2014, A&A, 572, A107
Lin D. N. C., Papaloizou J., 1979, MNRAS, 186, 799
Lin D. N. C., Papaloizou J., 1986, ApJ, 309, 846
Lin D. N. C., Bodenheimer P., Richardson D. C., 1996, Nature, 380, 606
Lodato G., Clarke C. J., 2004, MNRAS, 353, 841
Lodders K., 2003, ApJ, 591, 1220
Lupu R. E. et al., 2014, ApJ, 784, 27
McCrea W. H., Williams I. P., 1965, R. Soc. Lond. Proc. Ser. A, 287, 143
Machida M. N., Inutsuka S., Matsumoto T., 2010, ApJ, 724, 1006
Machida M. N., Inutsuka S.-i., Matsumoto T., 2011, ApJ, 729, 42
Marleau G.-D., Cumming A., 2014, MNRAS, 437, 1378
Marley M. S., Fortney J. J., Hubickyj O., Bodenheimer P., Lissauer J. J., 2007, ApJ, 655, 541
Marois C. T. et al., 2008, Science, 322, 1348
Mathis J. S., Rumpl W., Nordsieck K. H., 1977, ApJ, 217, 425
Matsuyama I., Johnstone D., Hartmann L., 2003, ApJ, 582, 893
Mayer L., Quinn T., Wadsley J., Stadel J., 2004, ApJ, 609, 1045
Michael S., Durisen R. H., Boley A. C., 2011, ApJ, 737, L42
Miller N., Fortney J. J., 2011, ApJ, 736, L29
Morbidelli A., Levison H. F., Gomes R., 2008, The Dynamical Structure of the Kuiper Belt and Its Primordial Origin. Univ. Arizona Press, Tucson, p. 275
Mordasini C., 2014, A&A, 572, A118
Mordasini C., Alibert Y., Benz W., 2009, A&A, 501, 1139
Nayakshin S., 2010a, MNRAS, 408, L36
Nayakshin S., 2010b, MNRAS, 408, 2381
Nayakshin S., 2011a, MNRAS, 410, L1
Nayakshin S., 2011b, MNRAS, 413, 1462
Nayakshin S., 2011c, MNRAS, 416, 2974
Nayakshin S., 2014, MNRAS, 441, 1380
Nayakshin S., 2015a, MNRAS, 446, 459
Nayakshin S., 2015b, MNRAS, 448, L25
Nayakshin S., Cha S.-H., 2012, MNRAS, 423, 2104
Nayakshin S., Cha S.-H., 2013, MNRAS, 435, 2099
Nayakshin S., Fletcher M., 2015, MNRAS, 452, 1654
Nayakshin S., Lodato G., 2012, MNRAS, 426, 70
Nayakshin S., Cha S.-H., Bridges J. C., 2011, MNRAS, 416, L50
Nayakshin S., Helled R., Boley A. C., 2014, MNRAS, 440, 3797
Ormel C. W., Klahr H. H., 2010, A&A, 520, A43
Paxton B., Bildsten L., Dotter A., Herwig F., Lesaffre P., Timmes F., 2011, ApJS, 192, 3
Petigura E. A., Marcy G. W., Howard A. W., 2013, ApJ, 770, 69
Pollack J. B., Hubickyj O., Bodenheimer P., Lissauer J. J., Podolak M., Greenzweig Y., 1996, Icarus, 124, 62
Rafikov R. R., 2005, ApJ, 621, L69
Rice W. K. M., Lodato G., Armitage P. J., 2005, MNRAS, 364, L56

Ritter H., 1988, A&A, 202, 93
Safronov V. S., 1972, Evolution of the protoplanetary cloud and formation of the earth and planets. Israel Program for Scientific Translations, Keter Publishing House, Jerusalem, Israel, p. 212
Shakura N. I., Sunyaev R. A., 1973, A&A, 24, 337
Shimaki Y., Arakawa M., 2012, Icarus, 221, 310
Stamenković V., Noack L., Breuer D., Spohn T., 2012, ApJ, 748, 41
Syer D., Clarke C. J., 1995, MNRAS, 277, 758
Tsiganis K., Gomes R., Morbidelli A., Levison H. F., 2005, Nature, 435, 459
Tsukamoto Y., Takahashi S. Z., Machida M. N., Inutsuka S.-i., 2015, MNRAS, 446, 1175
Vazan A., Helled R., 2012, ApJ, 756, 90
Vorobyov E. I., 2011, ApJ, 728, L45
Vorobyov E. I., Basu S., 2005, ApJ, 633, L137
Vorobyov E. I., Basu S., 2006, ApJ, 650, 956
Zhu Z., Hartmann L., Gammie C., 2009, ApJ, 694, 1045
Zhu Z., Nelson R. P., Dong R., Espaillat C., Hartmann L., 2012, ApJ, 755, 6

This paper has been typeset from a TEX/LATEX file prepared by the author.